

# Halide Perovskite Light-Emitting Diode Technologies

Kangyu Ji, Miguel Anaya,\* Anna Abfalterer, and Samuel D. Stranks\*

Halide perovskites have attracted considerable attention in next-generation solid-state lighting and displays owing to their outstanding optoelectronic properties. Over the past few years, perovskite light-emitting diodes (LEDs) have achieved high external quantum efficiencies of >20% with active layers showing photoluminescence quantum efficiencies close to unity. This paper reviews the historical breakthroughs and recent advancements in perovskite LEDs with near-infrared, red, green, and blue emission colors. Critical challenges, including device stability and material toxicity, are discussed. Finally, an outlook on white emission and lasing applications based on perovskite materials is presented.

## 1. Introduction

Since the first production in the 1960s, light-emitting diodes (LEDs) have only increased their importance in our everyday life, with prospects to replace every lamp and display given their more efficient use of energy, longer operational lifetimes, and versatility, among other reasons, in comparison to traditional light sources.<sup>[1]</sup> Recently, the reemergence of metal halide perovskites with a general formula of  $ABX_3$  (where A is a monovalent organic cation such as methylammonium (MA), formamidinium (FA), or an inorganic cation  $Cs^+$ , B is a metallic cation such as  $Pb^{2+}$  or  $Sn^{2+}$ , and X is a halide anion including  $I^-$ ,  $Br^-$ , or  $Cl^-$ ) has given rise to a new family of LEDs.<sup>[2]</sup> Their excellent electro-optical properties,<sup>[3,4]</sup> ease of processing, and versatility are particularly promising in optoelectronic applications.<sup>[5–7]</sup> Compared to traditional inorganic semiconductors such as gallium arsenide and indium gallium nitride, metal halide perovskites in general have more easily tunable bandgaps<sup>[8]</sup> and linewidths,<sup>[9]</sup> and low-temperature solution processability, which can offer high color quality, cost-effectiveness, and


flexibility for wearable technology, among other advantages.<sup>[7]</sup> Perovskite emitters can also be quantum-confined like quantum dots while still allowing adaption of multiple dimensions (such as quasi-2D perovskites) to obtain high emission yields while preserving charge injection,<sup>[10]</sup> as in organic LEDs (OLEDs). Negligible Stokes shifts<sup>[11]</sup> compared with typical OLEDs together with high photoluminescence quantum efficiencies (PLQEs) will potentially allow perovskite LEDs (PeLEDs) to surpass the existing power efficacies and other specifications.<sup>[12,13]</sup> For these reasons, halide perovskites can surmount the limitations of both traditional LEDs (suboptimal color quality) and emerging LEDs based on quantum dots (slow response time) and organic emitters (low maximum brightness) by producing bright, cost-effective, and high-color-purity LEDs.<sup>[14]</sup> Moreover, their thin-film character creates new opportunities to combine PeLEDs with nanostructured optical elements to achieve fine control over color and directionality of emission.<sup>[15–17]</sup>

PeLEDs were first demonstrated in the early 1990s based on layered 2D perovskite with large organic cations.<sup>[18–21]</sup> However, those devices were only operational at very low temperatures (<200 K) because near room temperature the electroluminescence (EL) efficiency dropped significantly owing to exciton quenching. The first PeLEDs incorporating 3D perovskite were reported in 2014, which operated at room temperature.<sup>[2]</sup> Since then, the development of PeLEDs has been highly influenced by well-established thin-film LED technologies based on organic and quantum dot emitters. The standard PeLED architectures and fabrication protocols are a legacy of their evolution from OLEDs, and many of the injection layers including 2,2',2''-(1,3,5-benzinetriyl)-tris(1-phenyl-1-H-benzimidazole) (TPBi) and poly(9,9-dioctylfluorene-*alt*-N-(4-*sec*-butylphenyl)-diphenylamine) (TFB) used in the field were developed for OLEDs.<sup>[22,23]</sup> The deposition of high optical quality films by solution process and thermal evaporation and synthetic methods such as contact doping and control over spatial confinement have also been influenced by previous works in thin-film LED technologies.<sup>[24,25]</sup> These collective insights have allowed the PeLED technology to evolve rapidly. Near-infrared and red PeLEDs were developed,<sup>[26]</sup> followed by efficient green PeLED as promising candidates to overcome the green gap in LEDs.<sup>[27]</sup> To date, the performance of blue-emitting PeLEDs is still lagging behind their red, green, and near-infrared analogues and is a key focus for the community, but important recent advances are encouraging. Together with new concepts developed for efficient blue emission and further performance enhancements in the green and red, extensive efforts are focusing on resolving the instability of this technology in

flexibility for wearable technology, among other advantages.<sup>[7]</sup> Perovskite emitters can also be quantum-confined like quantum dots while still allowing adaption of multiple dimensions (such as quasi-2D perovskites) to obtain high emission yields while preserving charge injection,<sup>[10]</sup> as in organic LEDs (OLEDs). Negligible Stokes shifts<sup>[11]</sup> compared with typical OLEDs together with high photoluminescence quantum efficiencies (PLQEs) will potentially allow perovskite LEDs (PeLEDs) to surpass the existing power efficacies and other specifications.<sup>[12,13]</sup> For these reasons, halide perovskites can surmount the limitations of both traditional LEDs (suboptimal color quality) and emerging LEDs based on quantum dots (slow response time) and organic emitters (low maximum brightness) by producing bright, cost-effective, and high-color-purity LEDs.<sup>[14]</sup> Moreover, their thin-film character creates new opportunities to combine PeLEDs with nanostructured optical elements to achieve fine control over color and directionality of emission.<sup>[15–17]</sup>

K. Ji, Dr. M. Anaya, A. Abfalterer, Dr. S. D. Stranks  
Cavendish Laboratory  
University of Cambridge  
19 JJ Thomson Avenue, Cambridge CB3 0HE, UK  
E-mail: ma811@cam.ac.uk; sds65@cam.ac.uk

Dr. M. Anaya, Dr. S. D. Stranks  
Department of Chemical Engineering and Biotechnology  
University of Cambridge  
Philippa Fawcett Drive, Cambridge CB3 0AS, UK

 The ORCID identification number(s) for the author(s) of this article can be found under <https://doi.org/10.1002/adom.202002128>.

© 2021 The Authors. Advanced Optical Materials published by Wiley-VCH GmbH. This is an open access article under the terms of the Creative Commons Attribution License, which permits use, distribution and reproduction in any medium, provided the original work is properly cited.

DOI: 10.1002/adom.202002128

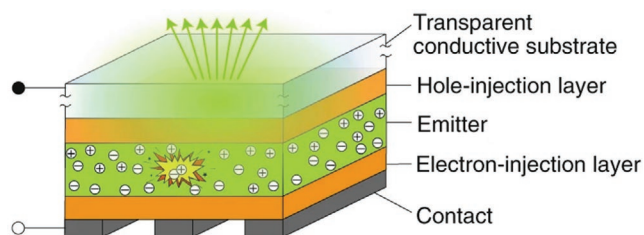


**Figure 1.** Schematic of an archetypical p-i-n PeLED. Note that the electron-injection and hole-injection layers can be interchanged to form an n-i-p architecture. Adapted with permission.<sup>[30]</sup> Copyright 2019, Springer Nature.

operando, which is caused by a series of processes, especially ion migration occurring in metal-halide perovskites under different stimuli and associated chemical reactions in the perovskite layers and at interfaces.<sup>[28,29]</sup> These undesirable effects are hindering the development of long-lifetime PeLEDs covering the entire visible spectrum, including yellow and orange, thus preventing their ultimate leap toward commercialization for both display and solid-state lighting technologies.

**Figure 1** shows a schematic representation of a typical PeLED device.<sup>[30]</sup> These devices are comprised of a glass substrate covered with a transparent conductive electrode such as fluorine-doped tin oxide (FTO) or indium-doped tin oxide (ITO). A perovskite emissive film is sandwiched between a hole-injecting layer (HIL) and an electron-injecting layer (EIL), where HIL and EIL also act as blocking barriers for electrons and holes, respectively. To close the device electrically, a thermally evaporated metallic film is typically used as the back contact. An external bias is applied to bring electrons and holes into the device under operation. The device architecture is designed in a way that electrons and holes (ideally) recombine radiatively in the perovskite emissive layer, giving rise to EL. While optimization of the perovskite emissive layer plays an important role in reaching high efficiency, proper band alignment, interfacial engineering, and outcoupling designs are crucial to further push the efficiency limit of PeLEDs.

In this review, we discuss the recent progress and development of PeLEDs covering different spectral ranges. We summarize key reports in the field leading to highly efficient PeLEDs through a series of strategies that have defined the standards in the community. We then discuss the challenges and outlook of PeLED technologies and present potential pathways toward white emission and lasing. We note that this review primarily focuses on electroluminescent LED technologies and does not extensively cover alternative light-emitting approaches including color-converting phosphors in which a highly emissive neat halide perovskite thin film is excited by an inorganic blue-emitting LED to generate high-quality green and red for displays, a very promising near-term commercial technology.<sup>[31]</sup>

## 2. Progress on Halide-Perovskite-Based LEDs

Understanding of the working principles of PeLEDs has been possible thanks to ongoing continuous feedback between the development of new synthesis routes of metal-halide perovskites, in-depth characterization of the materials, and device fabrication. This iterative process has, to date, led to emitting devices

that are becoming enticing for industry implementation into real-world applications such as displays. We note the importance of following unified characterization protocols to ensure the report of consistent LED metrics, allowing the identification of real breakthroughs in the field and accurate assessment of the technology readiness levels.<sup>[30]</sup> **Table 1** shows the most relevant examples of PeLEDs reported in the literature to date.

### 2.1. Early PeLEDs

The first bright near-infrared PeLEDs were fabricated from solution-processed halide perovskites by Tan et al. in 2014, as well as red and green PeLEDs with lower efficiencies.<sup>[2]</sup> In their work, a perovskite emitter was sandwiched between  $\text{TiO}_2/\text{Al}_2\text{O}_3$  (1 nm) and poly(9,9-di-*n*-octylfluorenyl-2,7-diyl) (F8), with ITO and  $\text{MoO}_3/\text{Ag}$  as the cathode and anode of the devices, respectively. A thin 15 nm 3D  $\text{MAPbI}_{3-x}\text{Cl}_x$  perovskite layer was made by spin-coating perovskite precursors in dimethylformamide (DMF) onto the  $\text{TiO}_2$  EIL followed by annealing—a method adapted from the processing of high-performance perovskite solar cells.<sup>[32]</sup> The thin perovskite layer acted as a quantum well to confine electrons and holes, improving radiative recombination over thicker-film analogs. Their infrared PeLED exhibited a maximum external quantum efficiency (EQE) of 0.76% and radiance of  $13.2 \text{ W sr}^{-1} \text{ m}^{-2}$  with EL peaking at 754 nm. It is worth mentioning that PeLEDs sharing typical solar cell configuration with solution-processed  $\text{TiO}_2$  EIL and Spiro-OMeTAD HIL (now injecting carriers instead of extracting them) were also demonstrated in the early stage, achieving a 0.48% EQE with an EL peak at 773 nm and a turn-on voltage as low as the perovskite bandgap ( $\approx 1.45 \text{ V}$ ).<sup>[33]</sup>

Fabrication of high-quality perovskite films is crucial for suppressing nonradiative recombination and improving the quantum efficiency of PeLEDs. Cho et al. reported that excess metallic Pb was present in perovskite films even with correct nominal stoichiometry in the precursor solutions because of the unintended loss of halide atoms or incomplete chemical reactions, resulting in increased nonradiative recombination in the perovskite.<sup>[34]</sup>  $\text{MAPbBr}_3$  perovskite films fabricated with excess MABr (MABr:PbBr<sub>2</sub> = 1.05:1) exhibited an enhanced external PLQE from 3% to 36%. Also, chloroform as an anti-solvent was used to wash away the precursor solvents (DMF and dimethyl sulfoxide (DMSO)), facilitating rapid crystallization of perovskite crystals and resulting in a uniform perovskite layer with small grain size. TPBi was introduced as an additive in the antisolvent to further reduce perovskite grain size. The reduction in perovskite grain size led to an  $\approx 2.8$  times enhancement in photoluminescence (PL) intensity. With both the stoichiometry modification and optimized nanograin engineering, they obtained green PeLEDs with an EQE of 8.53% and current efficiency of  $42.9 \text{ cd A}^{-1}$ . Meanwhile, excess CsBr was used in the first inorganic  $\text{CsPbBr}_3$  LEDs to reduce nonradiative recombination losses compared to control devices without excess CsBr (PL and EL in **Figure 2a,b**).<sup>[35]</sup> The 3D perovskite film was prepared by spin-coating CsBr and PbBr<sub>2</sub> in DMSO solvent and annealed at a relatively low temperature (70 °C). An EQE of 0.008% was achieved in the green PeLEDs based on this thin film, and the authors suggested there was

**Table 1.** Relevant reports of Pb-based PeLEDs according to their emission peak, alongside PLQE values of perovskite emitters measured in either solid film, blend film (mixed with organics/polymers), or solution. Perovskite compositions with unbalanced precursor stoichiometry are calculated assuming excess ions are not incorporated into lattice. Data values not explicitly reported are extracted from graphs. Pev in the device architecture refers to the perovskite emissive layer. PTAA = poly(triaryl amine); PC<sub>61</sub>BM = [6,6]-Phenyl-C<sub>61</sub>-butyric acid methyl ester; Liq = lithium 8-quinolate; TCTA = 4,4,4'-tris(carbazol-9-yl)triphenylamine; SOCP = PEDOT:PSS:PFI copolymer (PFI = tetrafluoroethylene-perfluoro-3,6-dioxo-4-methyl-7-octenesulfonic acid); TmPyPB = 1,3,5-tri(m-pyrid-3-yl-phenyl)benzene.

Perovskite emitter (near-infrared)	Morphology	PLQE [%]	Device architecture	EL [nm]	FWHM [nm]	EQE [%]	Radiance [W sr <sup>-1</sup> m <sup>-2</sup> ]	Turn-on voltage [V]	Publish date (year-month)	Ref.
MAPb(I/Cl) <sub>3</sub>	Film	26	ITO/TiO <sub>2</sub> /Al <sub>2</sub> O <sub>3</sub> /Pev/F8/MoO <sub>x</sub> /Ag	754	35	0.76	13.2	1.9	2014-08	[2]
MAPb(I/Cl) <sub>3</sub>	Film	–	ITO/ZnO/PEI/Pev/TFB/MoO <sub>x</sub> /Au	768	37	3.5	28	1.3	2015-02	[26]
MAPb(I/Cl) <sub>3</sub>	Film	–	FTO/TiO <sub>2</sub> /Pev/Spiro-OMeTAD/Au	773	42	0.48	7.1	1.5	2015-05	[33]
(PEA) <sub>2</sub> (MA) <sub>n-1</sub> Pb <sub>n</sub> I <sub>3n+1</sub>	Film	10	ITO/TiO <sub>2</sub> /Pev/F8/MoO <sub>x</sub> /Au	755	46	8.8	80	3.8	2016-06	[52]
(NMA) <sub>2</sub> (FA)Pb <sub>2</sub> I <sub>7</sub>	Film	60	ITO/ZnO:PEIE/Pev/TFB/MoO <sub>x</sub> /Au	786	47	9.6	55	1.5	2016-09	[53]
(NMA) <sub>2</sub> (FA)Pb <sub>2</sub> I <sub>6</sub> Br	Film	67	ITO/ZnO:PEIE/Pev/TFB/MoO <sub>x</sub> /Au	763	52	11.7	82	1.3	2016-09	[53]
FAPbI <sub>3</sub> NCs	Solution	>70	ITO/PEDOT:PSS/Pev/TPBi/LiF/Al	772	53	2.3	1.54	≥4.0	2017-03	[41]
(NMA) <sub>1.54</sub> (FA) <sub>1.46</sub> Pb <sub>2</sub> I <sub>7</sub>	Film	–	ITO/ZnO:PEIE/Pev/TFB/MoO <sub>x</sub> /Au	780	51	12.7	254	1.5	2018-02	[54]
FAPbI <sub>3</sub> + 5AVA	Blend film	70	ITO/ZnO:PEIE/Pev/TFB/MoO <sub>x</sub> /Au	803	40	20.7	390	1.3	2018-10	[60]
(NMA) <sub>2</sub> (FA)Pb <sub>2</sub> I <sub>7</sub> + quasi-3D + poly-HEMA	Blend film	96	ITO/MZO:PEIE/Pev/TFB+PFO/MoO <sub>x</sub> /Au	795	49	20.1	5	1.3	2018-11	[61]
FAPbI <sub>3</sub> + ODEA	Blend film	56	ITO/ZnO:PEIE/Pev/TFB/MoO <sub>x</sub> /Au	800	43	21.6	308	1.3	2019-03	[64]
Perovskite emitter (red)	Morphology	PLQE [%]	Device architecture	EL [nm]	FWHM [nm]	EQE [%]	Luminance [cd m <sup>-2</sup> ]	Turn-on voltage [V]	Publish date (year-month)	Ref.
MAPbBr <sub>2</sub> I	Film	–	ITO/PEDOT:PSS/Pev/F8/Ca/Ag	630	78	0.018	16.2	3.5	2014-08	[2]
CsPb(I/Br) <sub>3</sub> NCs + TMA	Film	–	ITO/ZnO/Pev/TFB/MoO <sub>x</sub> /Ag	619	29	1.4	1559	2.1	2016-03	[47]
CsPbI <sub>3</sub> NCs + TMA	Film	85	ITO/ZnO/Pev/TFB/MoO <sub>x</sub> /Ag	698	31	5.7	206	1.7	2016-03	[47]
CsPbI <sub>3</sub> NCs + IDA	Solution	95	ITO/PEDOT:PSS/poly-TPD/Pev/TPBi/LiF/Al	688	33	5.0	748	4.5	2017-12	[46]
CsPbI <sub>3</sub> NCs + Ag	Film	70	Ag/ZnO/PEI/Pev/TCTA/MoO <sub>3</sub> /Au/MoO <sub>3</sub>	690	36	11.2	1106	2.2	2018-06	[49]
CsPb(I/Br) <sub>3</sub> NCs	Solution	80	ITO/PEDOT:PSS/poly-TPD/Pev/TPBi/Liq/Al	653	33	21.3	500	2.8	2018-10	[50]
Perovskite emitter (green)	Morphology	PLQE [%]	Device architecture	EL [nm]	FWHM [nm]	EQE [%]	Luminance [cd m <sup>-2</sup> ]	Turn-on voltage [V]	Publish date (year-month)	Ref.
MAPbBr <sub>3</sub>	Film	7	ITO/PEDOT:PSS/Pev/F8/Ca/Ag	517	25	0.10	364	3.3	2014-08	[2]
MAPbBr <sub>3</sub>	Film	–	ITO/ZnO/PEI/Pev/TFB/MoO <sub>x</sub> /Au	532	22	0.80	20 000	2.2	2015-02	[26]
MAPbBr <sub>3</sub> + PIP	Blend film	–	ITO/PEDOT:PSS/Pev/F8/Ca/Ag	534	19	1.2	2000	3.1	2015-03	[27]
MAPbBr <sub>3</sub> + PEO	Blend film	–	ITO/Pev/In/Ga	532	23	0.17	4064	2.9	2015-08	[58]
CsPbBr <sub>3</sub>	Film	16	ITO/PEDOT:PSS/Pev/F8/Ca/Ag	527	18	0.008	407	3.0	2015-10	[35]
CsPbBr <sub>3</sub> NCs	Film	>85	ITO/PEDOT:PSS/PVK/Pev/TPBi/LiF/Al	516	23	0.12	946	4.2	2015-10	[43]
MAPbBr <sub>3</sub> NCs	Solution	92	ITO/PEDOT:PSS/Pev/TPBi/CsF/Al	524	24	1.1	2503	2.9	2015-12	[40]
MAPbBr <sub>3</sub>	Film	36	SOCP/Pev/TPBi/LiF/Al	540	20	8.5	15 000	3.0	2015-12	[34]
CsPbBr <sub>3</sub> NCs + TMA	Film	60	ITO/ZnO/Pev/TFB/MoO <sub>x</sub> /Ag	523	19	0.19	2335	2.7	2016-03	[47]
CsPbBr <sub>3</sub> + PEO	Blend film	60	ITO/PEDOT:PSS/Pev/TPBi/LiF/Al	521	21	4.3	53 525	2.5	2016-08	[59]
CsPbBr <sub>3</sub> NCs	Solution	92	ITO/PEDOT:PSS/poly-TPD/Pev/TPBi/LiF/Al	512	20	6.3	15 185	3.4	2016-11	[45]
(PEA) <sub>2</sub> (MA) <sub>4</sub> Pb <sub>5</sub> Br <sub>16</sub>	Film	60	ITO/PEDOT:PSS/Pev/TPBi/LiF/Al	526	24	7.4	8400	3.4	2017-05	[55]
Cs <sub>0.87</sub> MA <sub>0.13</sub> PbBr <sub>3</sub>	Film	55	ITO/ZnO/PVP/Pev/CBP/MoO <sub>3</sub> /Al	520	18	10.4	91 000	2.5	2017-06	[36]
(PEA) <sub>2</sub> (FAPbBr <sub>3</sub> ) <sub>n-1</sub> PbBr <sub>4</sub> + TOPO	Film	74	ITO/m-PEDOT:PSS/Pev/TPBi/LiF/Al	532	23	14.4	9120	3.0	2018-02	[57]
(PEA) <sub>2</sub> Cs <sub>n-1</sub> Pb <sub>n</sub> Br <sub>3n+1</sub> + organic	Film	70	ITO/poly-TPD/Pev/TPBi/LiF/Al	514	22	15.5	19 540	2.8	2018-09	[56]
CsPbBr <sub>3</sub> + MABr	Blend film	80	ITO/PEDOT:PSS/Pev/PMMA/B3PYMPM/LiF/Al	525	20	20.3	14 000	2.7	2018-10	[62]
CsPbBr <sub>3</sub> NCs	Solution	≈100	ITO/PEDOT:PSS/PTAA/Pev/TPBi/LiF/Al	508	17	22.0	10 000	2.5	2020-07	[80]

**Table 1.** Continued.

Perovskite emitter (blue)	Morphology	PLQE [%]	Device architecture	EL [nm]	FWHM [nm]	EQE [%]	Luminance [ $\text{cd m}^{-2}$ ]	Turn-on voltage [V]	Publish date (year-month)	Ref.
MAPbBr <sub>1.08</sub> Cl <sub>1.92</sub>	Film	–	ITO/PEDOT:PSS/Pev/PC <sub>61</sub> BM/Ag	482	20	$3 \times 10^{-4}$	1.7	3.4	2015-06	[66]
CsPb(Br/Cl) <sub>3</sub> NCs	Solution	–	ITO/PEDOT:PSS/PVK/Pev/TPBi/LiF/Al	455	20	0.07	742	5.1	2015-10	[43]
CsPb(Br/Cl) <sub>3</sub> NCs + TMA	Film	2	ITO/ZnO/Pev/TFB/MoO <sub>x</sub> /Ag	480	17	0.007	8.7	5.4	2016-03	[47]
CsPbBr <sub>3-x</sub> NCs	Solution	–	ITO/PEDOT:PSS/PVK/Pev/TPBi/LiF/Al	490	19	1.9	35	5.0	2016-08	[68]
2D MAPbBr <sub>3</sub> ( <i>n</i> = 3)	Film	>40	ITO/PEDOT:PSS/PVK/Pev/TPBi/LiF/Al	456	18	0.005	≈2	6.0	2016-10	[72]
2D MAPbBr <sub>3</sub> ( <i>n</i> = 5)	Film	>40	ITO/PEDOT:PSS/PVK/CBP/Pev/TPBi/LiF/Al	492	24	0.23	8.5	4.0	2016-10	[72]
Cs <sub>10</sub> (MA <sub>0.17</sub> FA <sub>0.83</sub> ) <sub>(100-x)</sub> Pb(Br/Cl) <sub>3</sub>	Film	–	ITO/ZnO/Pev/NPD/MoO <sub>x</sub> /Al	475	28	1.7	3567	3.2	2017-02	[67]
(EA) <sub>2</sub> (MA) <sub>n-1</sub> Pb <sub>n</sub> Br <sub>3n+1</sub>	Film	–	ITO/PEDOT:PSS/Pev/TmPyPB/CsF/Al	485	40	2.6	200	2.7	2017-08	[75]
CsPbBr <sub>3</sub> NPLs	Solution	96	ITO/PEDOT:PSS/poly-TPD/Pev/TPBi/LiF/Al	463	12	0.12	62	4.2	2018-07	[70]
(PEA) <sub>2</sub> (Cs/MA) <sub>1.5</sub> Pb <sub>2.5</sub> Br <sub>8.5</sub> + IPABr	Film	73	ITO/PEDOT:PSS/Pev/TPBi/LiF/Al	490	28	1.5	2480	5.5	2018-08	[74]
PBABr <sub>1.1</sub> (Cs <sub>0.7</sub> FA <sub>0.3</sub> PbBr <sub>3</sub> )	Film	60	ITO/NiO/TFB/PVK/Pev/TPBi/LiF/Al	483	26	9.5	700	3.5	2019-08	[78]
CsPbBr <sub>3</sub> NCs	Solution	≈100	ITO/PEDOT:PSS/PTAA/Pev/TPBi/LiF/Al	478	20	12.3	500	2.8	2020-07	[80]
(PEA) <sub>2</sub> (Cs <sub>0.4</sub> EA <sub>0.6</sub> PbBr <sub>3</sub> ) <sub>2</sub> PbBr <sub>4</sub>	Film	70	ITO/m-PEDOT:PSS/Pev/TPBi/LiF/Al	488	25	12.1	2191	3.0	2020-08	[79]
(PEA) <sub>0.4</sub> (DPPA) <sub>0.4</sub> Cs <sub>1.3</sub> PbCl <sub>1.1</sub> Br <sub>2.8</sub>	Film	60	ITO/PEDOT:PSS/TFB/Pev/TPBi/LiF/Al	473	22	8.8	482	3.0	2020-12	[77]
Rb <sub>0.07</sub> Cs <sub>0.8</sub> FA <sub>0.13</sub> PbBr <sub>1.8</sub> Cl <sub>1.2</sub>	Film	25	ITO/NiO <sub>x</sub> /PVK/PVP/Pev/TPBi/LiF/Al	477	18	11.0	2180	2.6	2021-01	[81]

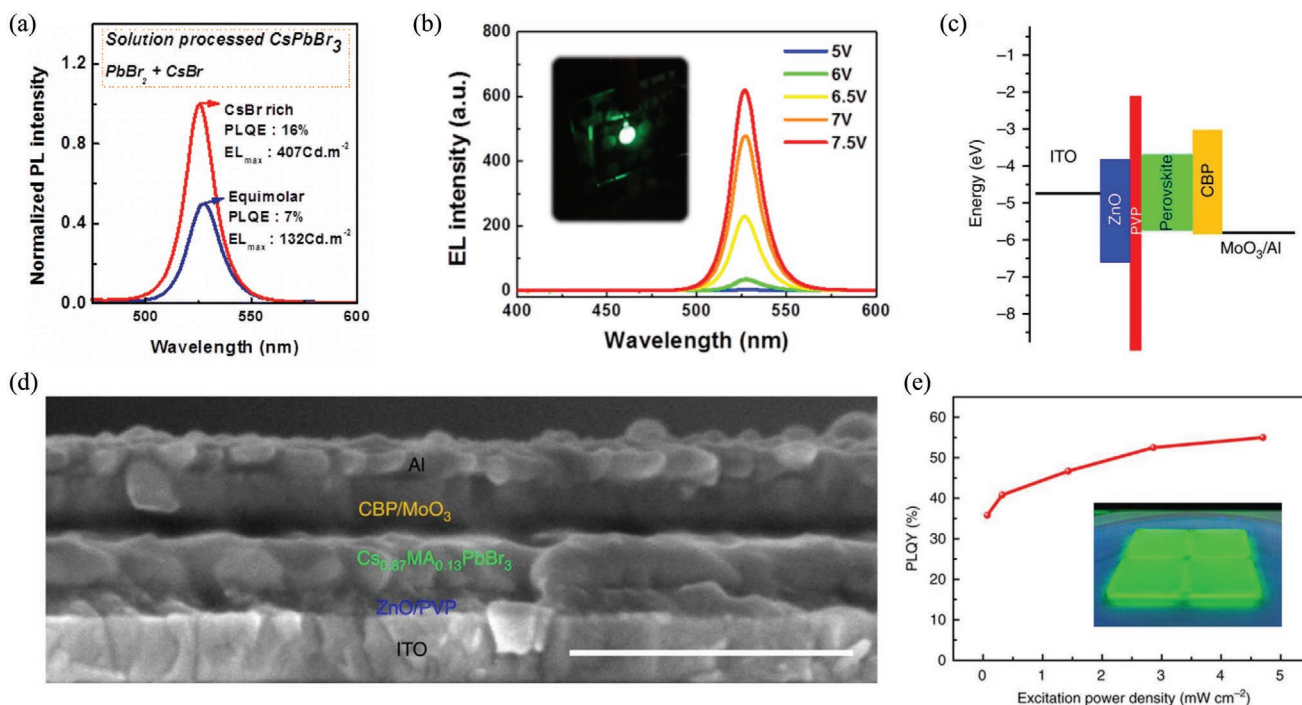


**Figure 2.** a) PL spectra of equimolar and CsBr-rich CsPbBr<sub>3</sub> films. Reproduced with permission.<sup>[35]</sup> Copyright 2015, American Chemical Society. b) EL spectra of LEDs based on CsBr-rich CsPbBr<sub>3</sub> at different driving voltages. Inset: the photograph shows a working PeLED. Adapted with permission.<sup>[35]</sup> Copyright 2015, American Chemical Society. c) Band alignment and d) cross-sectional SEM image of PeLEDs based on a Cs<sub>0.87</sub>MA<sub>0.13</sub>PbBr<sub>3</sub> film, scale bar is 500 nm. Reproduced with permission.<sup>[36]</sup> Copyright 2017, Springer Nature. e) PLQE of Cs<sub>0.87</sub>MA<sub>0.13</sub>PbBr<sub>3</sub> film as a function of excitation power density. Inset: PL image of perovskite films on ZnO/PVP under ultraviolet lamp excitation. Adapted with permission.<sup>[36]</sup> Copyright 2017, Springer Nature.

still ample room for performance improvement of inorganic PeLEDs.

Various interfacial engineering approaches have been explored to improve the quality of perovskite films and reduce the injection barrier. Wang et al. introduced a multifunctional polyethyleneimine (PEI) interlayer between the ZnO EIL and the perovskite emissive layer.<sup>[26]</sup> The hydrophilic nature of the PEI interlayer substantially improved the surface wetting property of the resulting EIL and thus enhanced the crystallinity and surface coverage of the perovskite film. Furthermore, the PEI layer lowered the work function of ZnO from 3.7 to 3.2 eV and facilitated electron injection into the perovskite layer, leading to a low turn-on voltage of 1.3 V. They also used TFB as a HIL and electron-blocking layer owing to its high hole mobility and high ionization potential. The combination of hole-blocking ZnO and electron-blocking TFB layers allowed efficient charge carrier confinement within perovskite layers. Their champion near-infrared PeLED device reached 3.5% EQE with a high radiance of  $28 \text{ W sr}^{-1} \text{ m}^{-2}$ . Zhang and co-workers demonstrated a similar approach to improve the perovskite film morphology.<sup>[36]</sup> They introduced a thin hydrophilic insulating polymer polyvinyl pyrrolidone (PVP) between the ZnO EIL and perovskite layer for better wetting of the perovskite precursors (Figure 2c,d). In addition, the researchers incorporated a small fraction of MA cation in the perovskite structure and developed green PeLED with the mixed-cation  $\text{Cs}_{0.87}\text{MA}_{0.13}\text{PbBr}_3$  composition. The perovskite film exhibited a high PLQE of 55% (Figure 2e). As a result, their devices achieved an EQE of 10.4% and high luminance of  $91\,000 \text{ cd m}^{-2}$ .

## 2.2. Perovskite Goes Small

Halide perovskite nanocrystals (NCs) exhibit high PLQE and narrow emission bandwidths, making them ideal for light-emitting applications.<sup>[37]</sup> Colloidal  $\text{MAPbX}_3$  NCs as green emitters in LEDs were first reported through reprecipitation or hot-injection-type methods.<sup>[38,39]</sup> Challenges with the purification of  $\text{MAPbX}_3$  NCs (separation of targeted product from the prepared solution) were overcome by Huang et al., who developed a nonaqueous emulsion synthesis,<sup>[40]</sup> where an emulsion system was created using two immiscible solvents (DMF and *n*-hexane), and a demulsifier was subsequently added into the solvent to control the crystallization process. They made monodisperse  $\text{MAPbBr}_3$  NCs with a peak PLQE of 92% in solution, and the green PeLEDs based on these NCs exhibited an EQE of 1.1% with a turn-on voltage of 2.9 V. In 2017, PeLEDs based on colloidal  $\text{FAPbI}_3$  NCs were demonstrated by Protesescu et al.<sup>[41]</sup> They reported a facile colloidal synthesis method for stable  $\text{FAPbI}_3$  NCs with a uniform mean size of 10–15 nm and PL emission peaks at 770–780 nm. With an  $\approx 30$  nm spin-coated layer of colloidal  $\text{FAPbI}_3$ , their devices exhibited an EL peak at 772 nm, a radiance of  $1.54 \text{ W sr}^{-1} \text{ m}^{-2}$ , and a maximum EQE of 2.3%.

The most promising and well-studied perovskite NCs for light-emitting applications are the inorganic  $\text{CsPbX}_3$  family. In 2015, colloidal synthesis of monodispersed inorganic  $\text{CsPbX}_3$  NCs was reported, where the PL of perovskite NCs could be tuned across the visible spectrum (410–700 nm) with a high

PLQE of 50–90%.<sup>[42]</sup> The first example of PeLEDs based on  $\text{CsPbBr}_3$  NCs was reported by Song et al.<sup>[43]</sup> The  $\text{CsPbBr}_3$  NCs could be stored for more than two months, showing higher stability compared to  $\text{MAPbBr}_3$  NCs, and the thin film exhibited a very high PLQE of >85%. Their perovskite emitter was sandwiched between 40 nm poly(3,4-ethylenedioxythiophene) polystyrene sulfonate (PEDOT:PSS) with 10-nm-thick poly(9-vinylcarbazole) (PVK) HILs and 40-nm-thick TPBi EIL. The PVK layer was used to reduce the hole injection barrier from PEDOT:PSS into the perovskite emissive layer. This strategy resulted in an effective recombination of charge carriers in the perovskite NC layer. Their champion green PeLEDs exhibited a moderate EQE of 0.12%, a luminance of  $946 \text{ cd m}^{-2}$  with a very narrow full width at half maximum (FWHM) of 23 nm, representing a promising starting point for inorganic PeLEDs.

However,  $\text{CsPbX}_3$  NCs suffer from chemical instability owing to the highly dynamic bonding between capping ligands and NC surface.<sup>[44]</sup> In addition, most of the common capping ligands (e.g., oleic acid, OA, and oleylamine, OLA) are not electrically conductive, preventing charge carrier injection into perovskite NCs.<sup>[45]</sup> A universal solution to these issues involves the search for passivation agents capable of conducting charges and stabilizing perovskite NCs at the same time. This is work still in progress in the field, but one simple and effective way to improve carrier injection is by controlling the number of ligands on the NC surface. An optimum ligand density between excessive ligands (poor carrier injection and transportation) and insufficient ligands (low PLQE and colloidal stability) was found by using a mixture of hexane and ethyl acetate (Figure 3a).<sup>[45]</sup> Benefitting from this approach, green PeLEDs with a peak EQE 6.3% were demonstrated with two-cycle-purified NCs (Figure 3b,c), remarkably higher than in previous reports.<sup>[40,42]</sup>

Pan et al. explored a novel ligand, 2,2'-iminodibenzoic acid (IDA), for NC surface passivation, leading to a stronger bonding of the ligand to the perovskite surface in comparison to OA.<sup>[46]</sup> They found that the double carboxylic groups in the IDA ligand could bind to two exposed Pb atoms at the  $\text{CsPbI}_3$  surface, resulting in a high surface binding energy which inhibited NC degradation to the yellow phase. Their IDA-treated  $\text{CsPbI}_3$  NC solution showed a high PLQE of 95%, remarkably higher than the untreated sample (80%). With PEDOT:PSS and poly(*N,N'*-bis-4-butylphenyl-*N,N'*-bisphenyl)benzidine (poly-TPD) as HIL and TPBi as EIL, their red PeLED exhibited EL emission at 688 nm with turn-on voltage at 4.5 V, a maximum EQE of 5.02%, and a luminance of  $748 \text{ cd m}^{-2}$ .

One practical issue that the fabrication of all solution-processed PeLEDs (except the evaporation of metal electrode) involves is the washing out of the perovskite NCs when other device layers are spin-coated on top. To overcome this challenge, a cross-linking approach can be considered to not only make the NC film stable against subsequent organic solvents but also to passivate the perovskite NC surface. By exposing the perovskite film under trimethylaluminum (TMA) vapor, Li et al. linked perovskite NCs together with a well-connected network of aluminum oxide, improving PLQE of the treated  $\text{CsPbI}_3$  films from 25% to 85%.<sup>[47]</sup> Their PeLEDs exhibited an EQE of 5.7% with EL emission at 698 nm and a luminance of  $206 \text{ cd m}^{-2}$ .

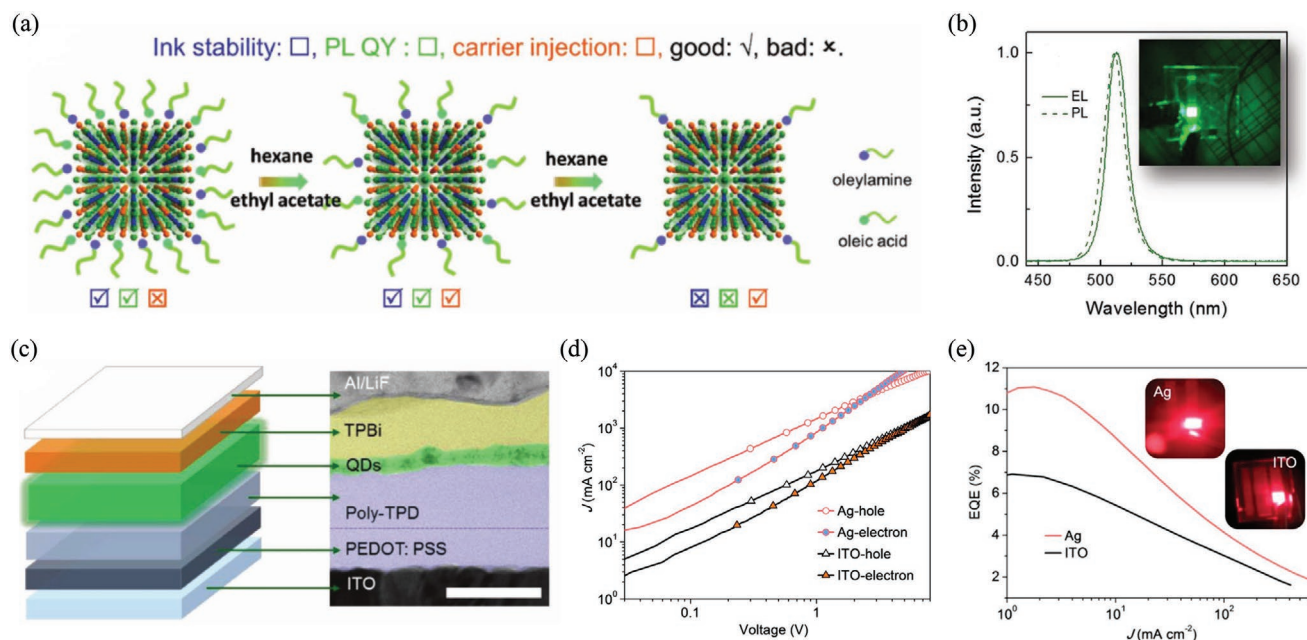


**Figure 3.** a) Schematic illustration of the control of ligand density on CsPbBr<sub>3</sub> NC surfaces and the corresponding changes of ink stability, PLQE, and carrier injection. b) Normalized EL spectra (solid lines) and PL spectra (dashed lines) of CsPbBr<sub>3</sub> PeLEDs with two purifying cycles. Inset: a photograph shows a working device (with an emitting area of 2 mm × 2 mm) at an applied voltage of 5 V. c) Schematic illustration and a cross-sectional TEM image (scale bar: 50 nm) showing the PeLED architecture. Reproduced with permission.<sup>[45]</sup> Copyright 2017, Wiley-VCH. d) Current density versus voltage curves of the “electron-only” and “hole-only” PeLEDs with Ag and ITO cathodes. e) EQE versus current density for PeLEDs with Ag and ITO cathodes; insets show photographs of the respective working devices. Reproduced with permission.<sup>[49]</sup> Copyright 2018, American Chemical Society.

Metal ion doping and passivation have also been applied to improve the stability and optical properties of perovskite NCs, later for example by suppressing trion-formation.<sup>[48]</sup> In 2018, Lu et al. replaced traditional ITO with an Ag cathode to reduce both electron and hole injection barriers in the PeLED structure (Figure 3d).<sup>[49]</sup> They reported spontaneous doping of Ag<sup>+</sup> ions from the cathode into the CsPbI<sub>3</sub> NC layer, where some of the Ag<sup>+</sup> ions formed AgI through reaction with I<sup>-</sup> ions at the NC surface, while the authors proposed others might enter the perovskite crystal lattice. Ag-doped CsPbI<sub>3</sub> film exhibited improved stability over time in both PL and EL with respect to their undoped counterparts, and the Ag/EIL/CsPbI<sub>3</sub> half-device structure showed a PLQE of 70% compared to 60% with ITO. Their best-performing red PeLED based on the Ag cathode reached an EQE of 11.2% with a peak luminance of 1106 cd m<sup>-2</sup> (Figure 3e).

However, CsPbI<sub>3</sub> NCs still exhibited lower stability compared to CsPbBr<sub>3</sub> NCs. Chiba et al. developed red PeLEDs from CsPbBr<sub>3</sub> by inducing Br<sup>-</sup>→I<sup>-</sup> anion exchange with ammonium iodine salts.<sup>[50]</sup> After replacing Br<sup>-</sup> anions in pristine CsPbBr<sub>3</sub> by I<sup>-</sup> anions, the perovskite NC films showed a red-shifted PL as expected, i.e., from 508 to 649 nm. They used long OLA cations during the anion-exchange process, which led to the desorption of OA ligands but increased the OLA ligand concentration and resulted in NCs exhibiting a higher PLQE of 80% compared to pristine CsPbBr<sub>3</sub> NCs (38%). Their red PeLEDs showed an outstanding EQE of 21.3% with high color purity. However, the highly efficient red PeLEDs exhibited a short operational lifetime of <1 h and a high operational voltage shift, which could be attributed to halide segregation

in the mixed-halide perovskite NCs.<sup>[51]</sup> Long-term operational stability of PeLEDs remains a big challenge for the research community.

### 2.3. Dimensional Control

Emerging 2D and quasi-2D Ruddlesden–Popper perovskites with quantum well structures have shown great advantages for the demonstration of stable and efficient PeLEDs. These systems benefit from the synergetic properties of purely confined perovskites (excellent thin-film quality and maximized emission) and pure bulk perovskites (good carrier injection and stability).<sup>[52]</sup> In 2016, Yuan et al. used multilayered quasi-2D perovskite materials by doping the MAPbI<sub>3</sub> perovskite precursor with phenylethylammonium (PEA, C<sub>6</sub>H<sub>5</sub>C<sub>2</sub>H<sub>4</sub>NH<sub>3</sub><sup>+</sup>).<sup>[52]</sup> The large ionic radius of the PEA cations forced the 3D perovskite network to separate into layered structures, with the number of PbI<sub>6</sub> monolayers,  $n$ , in the layered perovskite being controllable by adjusting the ratio of MAI to PEA. The quasi-2D perovskite film consisted of multiphase perovskite with different  $n$  values, and they showed that charge carriers funneled down to, and recombined on, the smallest bandgap domains through charge transfer cascades within the film. With a device architecture similar to the one reported by Tan et al.,<sup>[2]</sup> their champion near-infrared PeLEDs achieved an EQE of 8.8% with a radiance of 80 W sr<sup>-1</sup> m<sup>-2</sup>.

Wang et al. reported similar quasi-2D PeLEDs based on the addition of 1-naphthylmethylamine cations (NMA), reaching up to 60% PLQE in the (NMA)<sub>2</sub>(FA)Pb<sub>2</sub>I<sub>7</sub> perovskite films.<sup>[53]</sup> They applied an ultrathin layer of poly(ethylenimine)

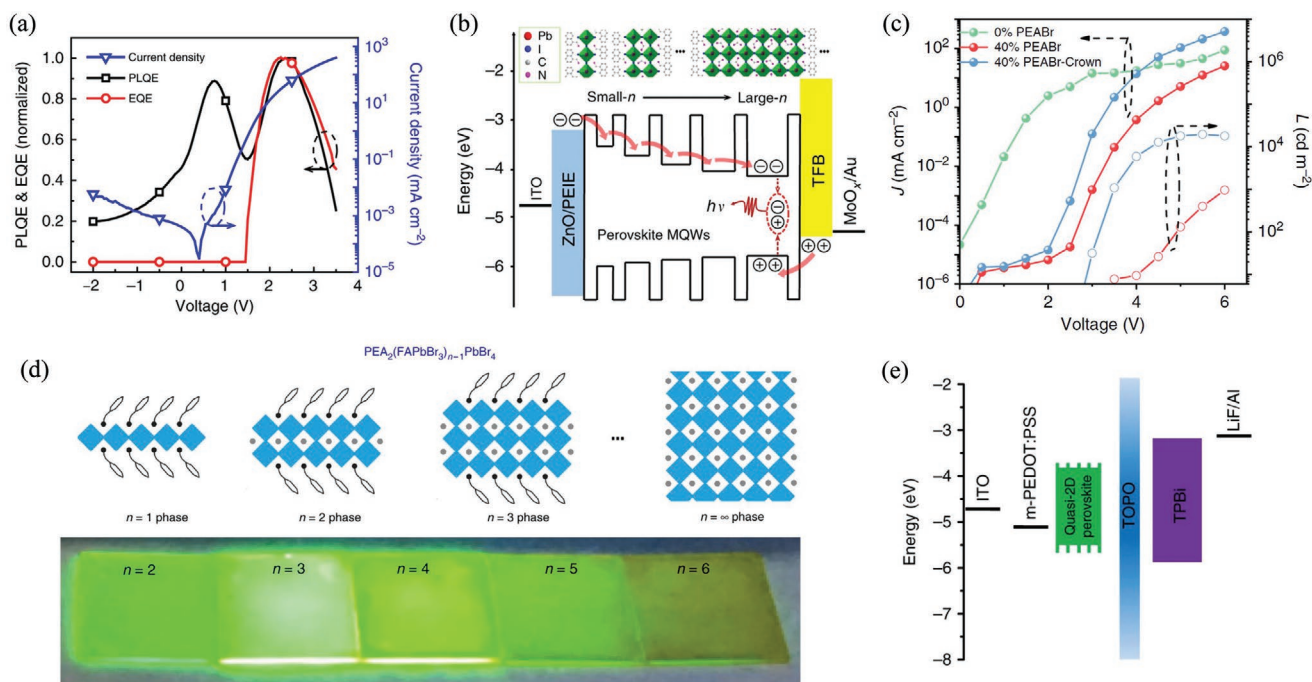


**Figure 4.** a) Dependence of current density (triangles), normalized PLQE (square), and EQE (circle) on the driving voltage. The PLQE and EQE were measured simultaneously on a working PeLED. b) Schematic representation of the flat-band energy level diagram and structures of the perovskite quasi-2D (multi-quantum-well) film which is an assembly of different layered lead halide perovskites with various  $n$  numbers. The quasi-2D structure enhances the probability of radiative recombination. Reproduced with permission.<sup>[54]</sup> Copyright 2018, Springer Nature. c)  $J$ - $V$ - $L$  data of devices based on the quasi-2D perovskite films with 0% PEABr, 40% PEABr, and with 40% PEABr-crown. Reproduced with permission.<sup>[56]</sup> Copyright 2018, Springer Nature. d) Top: scheme of  $\text{PEA}_2(\text{FAPbBr}_3)_{n-1}\text{PbBr}_4$  phases. The black part is PEA, the blue square is  $\text{PbBr}_6$  octahedron, and the gray dot is FA. Bottom: PL image of  $\text{PEA}_2(\text{FAPbBr}_3)_{n-1}\text{PbBr}_4$  films with different compositions under ultraviolet lamp excitation. Adapted with permission.<sup>[57]</sup> Copyright 2018, Springer Nature. e) Band alignment of each function layer in the PeLEDs. Reproduced with permission.<sup>[57]</sup> Copyright 2018, Springer Nature.

ethoxylated (PEIE) to reduce the work function of the ZnO EIL toward more suitable values. Their champion PeLEDs based on  $(\text{NMA})_2(\text{FA})\text{Pb}_2\text{I}_6\text{Br}$  film achieved a turn-on voltage of 1.3 V, a record EQE of 11.7%, and a maximum radiance of  $82 \text{ W sr}^{-1} \text{ m}^{-2}$  with an EL emission of 763 nm. Follow-up work by Zou et al. in 2018 found that both PL and EL responses decreased at high current densities (Figure 4a), which indicated that the EQE drop at high current densities was mainly caused by luminescence quenching.<sup>[54]</sup> By increasing the width of perovskite quantum wells (Figure 4b), they successfully suppressed the luminescence quenching in quasi-2D PeLEDs, raising the EQE to 12.7%. Their device EQE remained at  $\approx 10\%$  even at a high current density of  $500 \text{ mA cm}^{-2}$ .

Optimization of the phase domain distribution is crucial to achieving efficient PeLEDs built upon quasi-2D perovskite systems. By controlling the distribution of domains with different bandgaps, Quan et al. improved the energy transfer efficiency in quasi-2D perovskite films.<sup>[55]</sup> Through compositional and solvent engineering, they made films with a set of different domains where an excitation effectively transferred from a large population of high bandgap domains to a low number of low bandgap domains at a rate out-competing trapping minimized subsequent nonradiative recombination. With such a design strategy, the optimized film achieved an improved PLQE of 60% under low excitation densities of  $1.8 \text{ mW cm}^{-2}$ . With these materials, they demonstrated green PeLEDs with a peak EQE of 7.4% and a high luminance of  $8400 \text{ cd m}^{-2}$ . On

the other hand, Ban et al. added a small amount of an organic molecule (1,4,7,10,13,16-hexaoxacyclooctadecane) into a 2D  $\text{PEA}_2\text{Cs}_{n-1}\text{Pb}_n\text{Br}_{3n+1}$  film, resulting in more controlled phase separation between the organic and inorganic phases.<sup>[56]</sup> Their 2D nanoplatelet (NPLs) films exhibited a strong PLQE of 70%, and the related PeLEDs achieved low current leakage, a peak EQE of 15.5% (Figure 4c), and improved stability, where EQE maintained half of its initial value after  $\approx 90$  min of constant current density operation.

Compared to 3D perovskite, quasi-2D perovskites have smaller crystal sizes, which increase the concentration of trap states on the film surface and grain boundaries and result in low radiative recombination. To mitigate this issue, Yang et al. passivated the surface of  $\text{PEA}_2(\text{FAPbBr}_3)_{n-1}\text{PbBr}_4$  thin films with a small organic molecule, trioctylphosphine oxide (TOPO) (Figure 4d,e).<sup>[57]</sup> The PLQE of the best films ( $n = 3$ ) improved from 57% to 74% with a small PL redshift. They also modified the HIL with poly(sodium 4-styrenesulfonate) (PSS-Na) dopant to increase the work function for better hole injection. Through composition engineering and surface passivation, they achieved well-performing quasi-2D green PeLEDs with an EQE of 14.4%.

## 2.4. Perovskite Film Engineering

A well-thought-out design of the perovskite emissive layer through film engineering is necessary for realizing

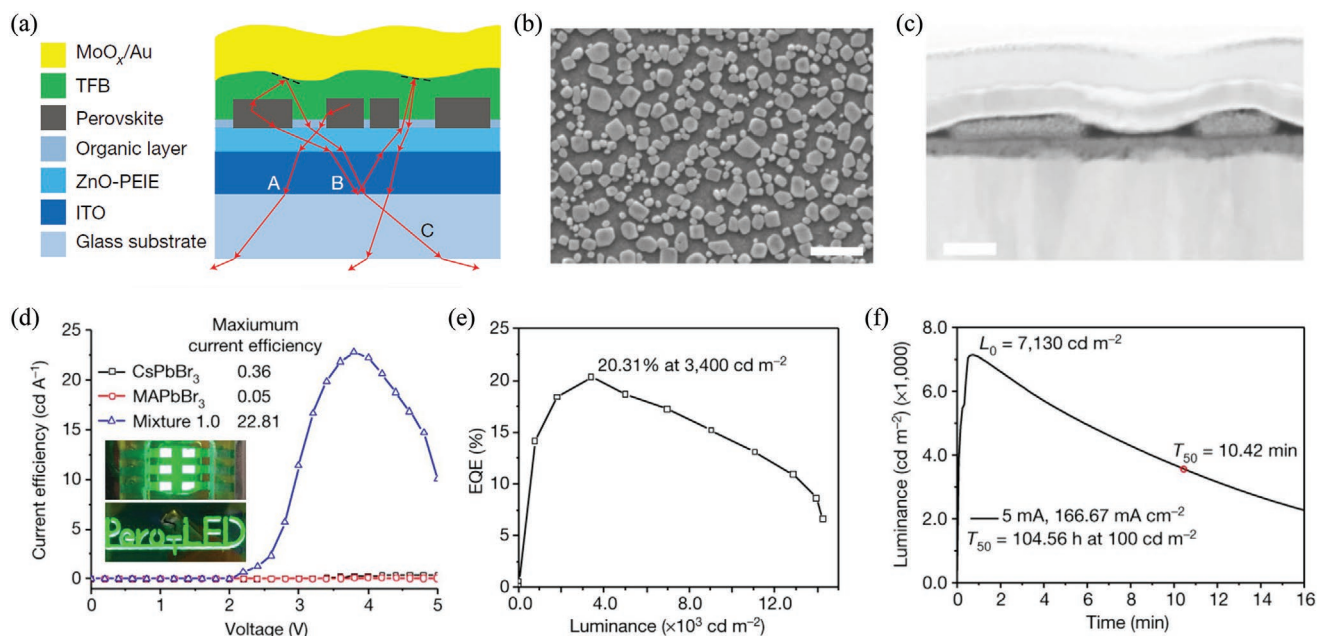


**Figure 5.** a) Schematic illustration of PeLEDs with sub-micrometer-structured perovskite emissive layer. Adapted with permission.<sup>[60]</sup> Copyright 2018, Springer Nature. b) SEM image of the perovskite film, the scale bar is 1 μm. c) Cross-section high-angle annular dark-field scanning electron microscope tomography image at high magnification, the scale bar is 100 nm. Reproduced with permission.<sup>[60]</sup> Copyright 2018, Springer Nature. d) Current efficiency–voltage curves of the three PeLEDs. Inset: photographs of PeLEDs fabricated with the mixture perovskite. Adapted with permission.<sup>[62]</sup> Copyright 2018, Springer Nature. e) EQE–L characteristics of the best-performing PeLEDs. f) Lifetime measurements of the best-performing mixture PeLED device. A constant driving current of 5 mA (167 mA cm<sup>-2</sup>) led to the luminance increasing from 3800 to 7130 cd m<sup>-2</sup> (L<sub>0</sub>) and then diminishing. This device's half-lifetime at 100 cd m<sup>-2</sup> is estimated to be about 104.56 h. Reproduced with permission.<sup>[62]</sup> Copyright 2018, Springer Nature.

high-performing PeLEDs to: i) reduce nonradiative recombination at the perovskite/injection layer interfaces, and ii) ensure efficient carrier injection. MA-based perovskites tend to form rough and nonuniform films when solution deposited as ultrathin layers of <50 nm, leading to a substantial current leakage in PeLEDs. Li et al. embedded perovskites into a perovskite/polymer matrix to mitigate this problem.<sup>[27]</sup> They mixed the perovskite precursor with a commercial aromatic polyimide (PIP), a transparent and insulating polymer suitable to be used as a charge-blocking material in LEDs. After spin-coating, emissive perovskite NCs were uniformly distributed within a thin matrix of dielectric PIP polymer. The PIP polymer formed a pinhole-free charge-blocking layer, and nonradiative current losses (via uncovered pinholes of perovskite NCs) could therefore be mitigated by the insulating PIP layer. The PIP-modified green PeLED structure exhibited an improved EQE of 1.2% in comparison to the 0.01% EQE obtained in devices without PIP. In the same year, green PeLEDs based on a composite thin film of perovskite/poly(ethylene oxide) (PEO) with a peak EQE of 0.17% were demonstrated.<sup>[58]</sup> The PEO polymer improved the morphology of the emissive layer and enhanced the ionic conductivity of the composite film, resulting in a moderate turn-on voltage of 2.9 V and a luminance of 4064 cd m<sup>-2</sup> in PeLEDs.

Like MA-based PeLEDs, the low efficiency of CsPbBr<sub>3</sub> analogues came from high leakage current owing to its incomplete surface coverage. In 2016, Ling et al. introduced a small amount of PEO polymer in the perovskite precursor solution to reduce pinholes in the perovskite films.<sup>[59]</sup> The CsPbBr<sub>3</sub>-PEO film exhibited a high PLQE of 60% owing to the surface passivation of PEO additives and smaller microcrystalline domains.

Thus, they achieved an EQE of 4.26% and high luminance of >50 000 cd m<sup>-2</sup> in their green PeLEDs.

In addition, the optical outcoupling from perovskite devices could be enhanced via film engineering. Cao et al. demonstrated efficient light extraction from their solution-processed perovskite with sub-micrometer-scale structures.<sup>[60]</sup> They used 5-aminovaleric acid (5AVA) additives in perovskite precursors to form perovskite films with α-phase FAPbI<sub>3</sub> platelets of sub-micrometer size. They showed that a dehydration reaction happened between 5AVA and PEIE-modified ZnO, resulting in an insulating organic layer that prevented current leakage from low surface coverage of the perovskite layer (Figure 5a–c). Benefiting from the concave-convex morphology where discrete perovskite platelets are embedded in a roughly 8-nm-thick organic layer, the perovskite film was able to emit wide-angle light with a high PLQE of 70%, and the PLQE remained high at 50% even at low laser excitation of 0.1 mW cm<sup>-2</sup>. Moreover, the amino-acid additives passivated surface defects of the perovskite materials and thus enhanced the emission properties of perovskites. As a result, their best PeLEDs exhibited a low turn-on voltage at 1.25 V, a peak EQE of 20.7%, and a high radiance of 390 W sr<sup>-1</sup> m<sup>-2</sup>.

Zhao et al. explored film engineering to enhance radiative recombination in near-infrared PeLEDs using a perovskite/polymer heterostructure.<sup>[61]</sup> They combined quasi-2D/3D perovskites with a wide-gap polymer poly(2-hydroxyethyl methacrylate) (poly-HEMA) to form a perovskite-polymer bulk heterostructure, which exhibited a strong external PLQE of 96% under 532 nm laser excitation. Through transient optical measurements, they found that localized higher-energy excitations



rapidly transformed into charge carriers at lower-energy sites within  $\approx 1$  ps, which is significantly faster than the energy funneling time of about 100 ps reported for quasi-2D/3D perovskites. Owing to the ultrafast excitation transfer, they observed negligible nonradiative recombination at the charge-injecting layer interfaces. The perovskite-polymer film also exhibited a lower refractive index of 1.9 than the value of 2.7 for standard halide perovskites, which improved the optical outcoupling from the emitter. Their device architecture included a 20-nm PEIE-modified magnesium-alloyed zinc oxide (MZO) as an EIL, a 180-nm-thick perovskite-polymer emissive layer, and a 50-nm-thick TFB layer blended with poly(9,9-di-*n*-octylfluorenyl)2,7-diyl (PFO) as a tunable HIL. They obtained a record EQE of 20.1% with their near-infrared PeLEDs and a turn-on voltage of 1.3 V, and the operation half-life of encapsulated devices reached 46 h.

Defect passivation has become an attractive strategy to obtain well-performing perovskite emitters.<sup>[62,63]</sup> Inspired by amino acid passivation approaches, Xu et al. designed new passivation molecules 2,2'-[oxybis(ethylenoxy)]diethylamine (ODEA) with improved interaction with perovskite defect sites.<sup>[64]</sup> They achieved a substantial decrease in nonradiative recombination in the perovskite films, boosting PLQE up to 56%. Consequently, the fabricated PeLEDs with FAPbI<sub>3</sub>/ODEA film in the molar ratio of 1:0.125 showed a high EQE of 21.6% and a high radiance of 308 W sr<sup>-1</sup> m<sup>-2</sup> at 3.3 V.

Lin et al. developed a quasi-core/shell structure consisting of the CsPbBr<sub>3</sub> emissive layer and MABr capping layer, where the MABr shell passivates nonradiative defects in CsPbBr<sub>3</sub> crystals and balances charge injection in the PeLEDs.<sup>[62]</sup> They further improved the charge balance by depositing a thin poly(methyl methacrylate) (PMMA) layer on top of the perovskite film, which enabled charge injection into the perovskite via tunneling. They also applied a 40-nm-thick 4,6-Bis(3,5-di(pyridin-3-yl)phenyl)-2-methylpyrimidine (B3PYMPM) layer as an EIL instead of the more standard TPBi in their PeLED structure. With those device optimizations, they achieved PeLEDs with a narrow green emission and a record EQE of 20.3% with a peak luminance of 14 000 cd m<sup>-2</sup> (Figure 5d–f).

## 2.5. Breaking the Blue Wall

The development of blue PeLEDs has been lagging behind their green, red, and infrared counterparts. As the blue color is an essential building block for full-color display and solid-state lighting applications, extensive efforts in the field have been dedicated to advancing this bottleneck technology. In 2015, Sadhanala et al. developed mixed Cl–Br PeLEDs with a tunable EL emission of 425–570 nm.<sup>[65]</sup> However, these devices with chloride content only emitted below 200 K. Kumawat et al. demonstrated the first blue PeLEDs working at room temperature with mixed-halide 3D perovskite MAPbBr<sub>1.08</sub>Cl<sub>1.92</sub>.<sup>[66]</sup> However, these PeLEDs had poor charge carrier balance which resulted in a low EQE of  $3 \times 10^{-4}\%$  and luminance of 2 cd m<sup>-2</sup> (Figure 6a). It is possible that pinholes present in the perovskite emissive layer may have acted as nonradiative recombination pathways in the device.

Through interfacial engineering, blue PeLEDs with triple cation perovskite films of Cs<sub>10</sub>(MA<sub>0.17</sub>FA<sub>0.83</sub>)<sub>(100-x)</sub>PbBr<sub>1.5</sub>Cl<sub>1.5</sub> were developed by Kim et al. in 2017,<sup>[67]</sup> where 100–*x* represented the content of MA and FA after Cs doping. Their

perovskite film exhibited excellent surface coverage and a sharp EL emission at 475 nm with 28 nm FWHM. The ZnO EIL and *N,N'*-bis(1-naphthyl)-*N,N'*-diphenylbenzidine ( $\alpha$ -NPD) HIL in their devices offered negligible energy offsets with the perovskite layer, resulting in efficient radiative recombination by confined carrier injection into perovskite (Figure 6b). With balanced charge injections and reduced nonradiative recombination at interfaces, their devices reached a peak EQE of 1.7% and luminance of 3567 cd m<sup>-2</sup>.

Blue PeLEDs based on perovskite NCs were demonstrated by Song et al. in 2015 with inorganic mixed halide perovskite CsPb(Br<sub>1-x</sub>Cl<sub>x</sub>)<sub>3</sub> made from a hot injection method.<sup>[43]</sup> With PEDOT:PSS and PVK as HILs and TPBi as an EIL, their devices achieved a peak EQE of 0.07% and a turn-on voltage of 5.1 V. Pan et al. replaced OA and OLA long ligands at the perovskite surface with a short mixed halide-ion pair ligand di-dodecyl dimethyl ammonium bromide chloride through ligand exchange and thus developed more efficient sky-blue PeLEDs based on mixed halide NCs, which exhibited an EQE of 1.9% and a luminance of 35 cd m<sup>-2</sup> with EL emission peaked at 490 nm.<sup>[68]</sup> The authors proposed that the use of halide-ion-pair ligands for passivation significantly improved the charge carrier balance of their devices.

However, LEDs based on mixed halide perovskite NCs are limited by halide phase segregation, resulting in shifts of EL/PL peaks and the formation of defects as the device operates.<sup>[47]</sup> To achieve long-term device stability, one way is to use perovskite NPLs with a 2D-confined structure.<sup>[69]</sup> PeLEDs based on CsPbBr<sub>3</sub> NPLs were demonstrated by Wu et al. with an EQE of 0.12% and a luminance of 62 cd m<sup>-2</sup>,<sup>[70]</sup> where Br vacancies at the surface of NPLs were passivated by an introduction of a small amount of HBr aqueous solution during the fabrication process (Figure 6c), which improved film PLQE from 18% to 96%. However, the EL peak of their devices was still redshifted owing to the aggregation of NPLs under bias. Therefore, new passivation methods are needed to improve the stability of NPLs and facilitate charge carrier injection into the NPL emissive layer. Regarding the latter, Hoye et al. have identified that the deep ionization potentials of perovskite NPLs could lead to a poor interface between the perovskite emissive layer and the HIL, which quenches excitations on the perovskite layer and limits charge injection into perovskite, thus compromising the performance of the PeLEDs.<sup>[71]</sup>

Examples of blue PeLEDs based on 2D perovskite with MAPbX<sub>3</sub> films were reported by Kumar et al. with tunable emissions from green to blue and high PLQEs of 40–90% (Figure 6d).<sup>[72]</sup> 2D perovskite was dispersed in an organic host 4,4'-bis(*N*-carbazolyl)-1,1'-biphenyl (CBP) and near-field Förster resonance energy transfer (FRET) between the host (donor) and the 2D perovskite material (acceptor) was created (Figure 6e), which enhanced device efficiencies. The best sky-blue (*n* = 5) PeLEDs showed an EQE of 0.23% with a luminance of 8.5 cd m<sup>-2</sup>.

Quasi-2D perovskite with proper bandgap tuning has also shown its potential in blue emission. In 2016, PeLEDs based on layered (PEA)<sub>2</sub>PbBr<sub>4</sub> with EL at 410 nm were demonstrated by Liang et al. with enhanced efficiency.<sup>[73]</sup> This was achieved by converting quasi-2D polycrystalline perovskite films to micrometer-sized 2D NPLs through a DMF vapor annealing method, leading to an EQE of 0.04% in devices. Apart from converting quasi-2D to 2D perovskite, however, the presence of impurities

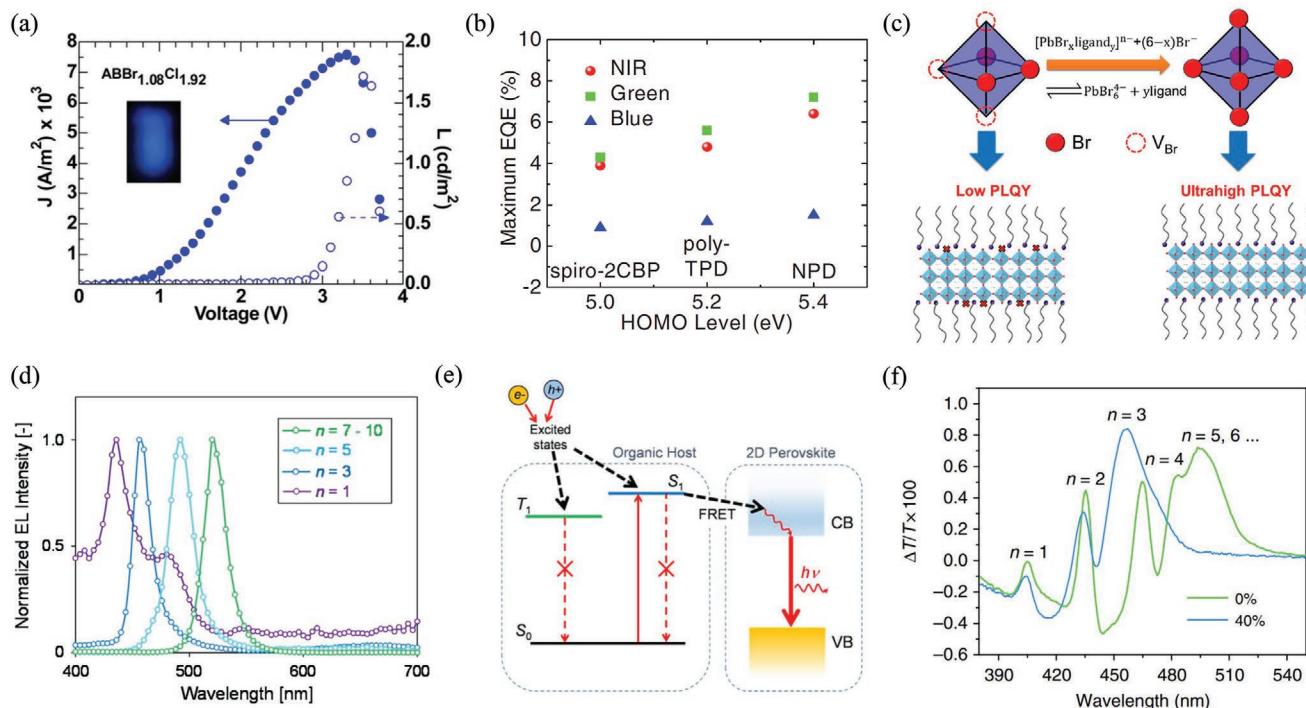


**Figure 6.** a)  $J$ - $V$ - $L$  characteristics of blue PeLEDs based on 3D  $\text{MAPb}(\text{Br}_{1-x}\text{Cl}_x)_3$  with insets of the operational LED picture. Reproduced with permission.<sup>[66]</sup> Copyright 2015, American Chemical Society. b) Maximum EQE of NIR-, green-, and blue-emission PeLEDs using various HTLs. Reproduced with permission.<sup>[67]</sup> Copyright 2017, Wiley-VCH. c) Schematic demonstration of Br vacancy passivation in  $\text{PbBr}_6^{4-}$  octahedra with an HBr complex solution. Adapted with permission.<sup>[70]</sup> Copyright 2018, American Chemical Society. d) EL spectra for PeLEDs using 2D  $\text{MAPbBr}_3$  perovskite colloidal solutions of  $n = 7-10$ ,  $n = 5$ ,  $n = 3$ , and  $n = 1$ . e) Schematic of FRET occurring at the interface between the organic host and 2D perovskite, in which the singlet excitons in the host transferred to the conduction band (CB) of 2D perovskite. Reproduced with permission.<sup>[72]</sup> Copyright 2016, American Chemical Society. f) TA spectra of  $\text{PEA}_2\text{A}_{1.5}\text{Pb}_{2.5}\text{Br}_{8.5}$  ( $\text{A} = \text{MA}$  and  $\text{Cs}$ ) with 0% and 40% IPABr additive, where  $n$  is the number of inorganic layers. Reproduced with permission.<sup>[74]</sup> Copyright 2018, Springer Nature.

with lower bandgap phases often caused PEA-based quasi-2D perovskite with pure Br halide content to shift toward green emission. As energy funneled from the higher bandgap phase to the lower bandgap phase, recombination mainly occurred at the lowest bandgap, which generated green instead of blue lights.<sup>[55]</sup> To solve this, Xing et al. replaced long PEA ligands with short iso-propylammonium (IPA) ligands to prevent nucleation of high  $n$  phases.<sup>[74]</sup> Their quasi-2D film had pure and monodisperse  $n = 2, 3$ , and 4 phases (Figure 6f) with a high PLQE of 88% and a stable PL at 477 nm. They demonstrated sky-blue PeLEDs with a peak EQE of 1.5% and a luminance of  $2480 \text{ cd m}^{-2}$  at 490 nm. Introducing ethylammonium bromide to quasi-2D  $\text{MAPbBr}_3$  had also achieved blue emission.<sup>[75]</sup> With the passivation of large ammonium bromides, those PeLEDs exhibited an EQE of 2.6% and a luminance of  $200 \text{ cd m}^{-2}$ . Adding the amino acid molecule,  $\gamma$ -aminobutyric acid, into the perovskite precursor has also shown to suppress the growth of larger- $n$  quantum wells while providing passivation on perovskite surface.<sup>[76]</sup> In addition to controlling the large- $n$  phases, Wang et al. used mixed ligands of PEA and 3,3-diphenylpropylamine (DPPA) to suppress perovskite formation of small- $n$  phases and concentrated quasi-2D phases on a narrower distribution with mainly  $n = 4$  domains, which reduced nonradiative recombination and improved charge transfer within the films.<sup>[77]</sup> Their devices based on such films achieved a

maximum EQE of 8.8% with a peak luminance of  $482 \text{ cd m}^{-2}$  at 473 nm.

However, the quasi-2D perovskite films for blue emission had poor charge injection properties. In 2019, Liu et al. developed blue PeLEDs with a record EQE of 9.5% using a mixed perovskite with quantum-confined NCs and quasi-2D phases.<sup>[78]</sup> By using an antisolvent processing technique to dissolve excess organic cations in the perovskite film, charge injection into the perovskite emissive layer was improved, and nonradiative recombination was suppressed. Thus, their blue PeLEDs reached a maximum luminance of  $700 \text{ cd m}^{-2}$ , a turn-on voltage of 3.5 V, and a peak EQE of 9.5%. Using PSS-Na modified PEDOT:PSS to increase work function has also been reported to facilitate hole injection by forming better band alignment with the quasi-2D perovskite.<sup>[57,79]</sup> Benefitting from this, Chu et al. demonstrated quasi-2D PeLEDs based on ethylammonium ( $\text{EA}$ ,  $\text{CH}_3\text{CH}_2\text{NH}_3^+$ )-incorporated perovskite films with tunable green-to-blue emission, and their sky-blue devices achieved 12.1% EQE at 488 nm with constant color output over 12 min of operation.<sup>[79]</sup>

Recently, the efficiency record of blue PeLEDs was set by Dong et al. using strongly confined perovskite NCs.<sup>[80]</sup> Perovskite NCs typically suffer from instability during ligand exchange and loss of efficiency through nonradiative recombination owing to surface defects. Dong et al. successfully stabilized perovskite NCs through a two-step ligand exchange:

first isopropyl-ammonium bromide (IPABr) was introduced to form a Br-rich surface of perovskite, then NaBr solution was added to replace the ammonium group with Na<sup>+</sup> ions. Thus, the positively charged outer shell with Na<sup>+</sup> was electrostatically adsorbed to the negatively charged inner shell, which lowered the trap density of the NCs and increased carrier mobility to  $\geq 0.01 \text{ cm}^2 \text{ V}^{-1} \text{ s}^{-1}$ . Their stable perovskite NCs showed near-unity PLQEs, and the blue PeLEDs achieved an EQE of 12.3% with 478 nm EL emission and a 2.8 V turn-on voltage. Their green PeLEDs also exhibited a remarkable efficiency of 22%. On the other hand, spectrally stable blue PeLEDs based on mixed Br-Cl perovskite were demonstrated by Karlsson et al., which had tunable emission from 451 to 490 nm with different halide ratios.<sup>[81]</sup> The perovskite films were prepared using a vapor-assisted crystallization method—the as-casted films were treated with a DMF atmosphere before annealing. This prolonged halide rearrangement within the perovskite films, which homogenized halide distribution and thus improved color stability of devices. Their blue PeLEDs achieved an EQE of 11.0% with EL peaks at 477 nm and a maximum luminance of  $2180 \text{ cd cm}^{-2}$ .

## 2.6. Beyond Pb-Based PeLEDs

Concerns about the toxicity of Pb-based halide perovskites in connection with potential real-world applications have in recent years led to the development of lead-free, perovskite-inspired materials. Although these novel light emitters and devices are yet in their infancy, they have demonstrated emission colors across the whole visible/infrared electromagnetic spectrum and ever-improving device integration.

For blue emission, Ma et al. fabricated LEDs with Cs<sub>3</sub>Sb<sub>2</sub>Br<sub>9</sub> quantum dots as the active material, achieving an EQE of 0.21% with an emission wavelength of 408 nm.<sup>[82]</sup> Additionally, Jun et al. accomplished EL originating from air-stable, lead-free Cs<sub>3</sub>Cu<sub>2</sub>I<sub>5</sub>, which has a large excitonic binding energy ( $\approx 490 \text{ meV}$ ).<sup>[83]</sup> Those Cs<sub>3</sub>Cu<sub>2</sub>I<sub>5</sub>-based LEDs emitted at a peak wavelength of  $\approx 440 \text{ nm}$  though reached a maximum luminance of only  $\approx 10 \text{ cd m}^{-2}$ . Chen et al. fabricated Cs<sub>3</sub>Cu<sub>2</sub>I<sub>5</sub>-poly-HEMA thin film-based LEDs with  $140 \text{ cd m}^{-2}$  peak luminance and just 0.27% EQE, despite near-unity PLQE values of as-prepared Cs<sub>3</sub>Cu<sub>2</sub>I<sub>5</sub> thin films.<sup>[84]</sup> For the corresponding Cs<sub>3</sub>Cu<sub>2</sub>I<sub>5</sub> NCs, Wang et al. demonstrated LEDs operating at 445 nm emission, with maximum EQE and luminance values of  $\approx 1.12\%$  and  $262.6 \text{ cd m}^{-2}$ , respectively.<sup>[85]</sup> Yet, the PL line width of the Cs<sub>3</sub>Cu<sub>2</sub>I<sub>5</sub> NCs remained broad at  $\approx 63 \text{ nm}$ , owing to self-trapped excitonic emission, while the LED showed an encouraging record half-life of  $\approx 108 \text{ h}$ . Self-trapped excitons are known to occur in polar semiconductors with strong exciton–phonon interaction, where the free exciton can trap in a pure, unperturbed crystal lattice.<sup>[86]</sup> Owing to their intrinsic broadband emission,<sup>[87]</sup> such self-trapped excitonic emitters may be less suitable for LED applications that require narrow emission linewidths. Furthermore, the loss of excitation energy to phonons, as indicated by the large Stokes shift for such materials, is undesirable.

Additionally, green PeLEDs based on [Ph<sub>4</sub>P]<sub>2</sub>[MnBr<sub>4</sub>] (Ph<sub>4</sub>P = tetraphenylphosphonium) were reported.<sup>[88]</sup> The devices emitted at  $\approx 520 \text{ nm}$  and reached a luminance of  $401 \text{ cd m}^{-2}$  and an EQE of 7.2%. For orange EL, an LED with peak emission at 625 nm (FWHM 162 nm), with 0.1% EQE, and maximum luminance

of  $350 \text{ cd m}^{-2}$  was developed using a 2D (C<sub>18</sub>H<sub>35</sub>NH<sub>3</sub>)<sub>2</sub>SnBr<sub>4</sub> material, whose emission is ascribed to intrinsic self-trapped states.<sup>[89]</sup> Similarly, also the yellow, broad EL from CsCu<sub>2</sub>I<sub>3</sub> is ascribed to self-trapped states.<sup>[90–92]</sup> Roccanova et al. carried out preliminary attempts to fabricate LEDs using CsCu<sub>2</sub>I<sub>3</sub>.<sup>[90]</sup> 1,3-bis(N-carbazolyl)benzene served as a host for the CsCu<sub>2</sub>I<sub>3</sub> additive, which was deposited by vacuum thermal evaporation. These LEDs showed EL peaking at 554 nm (with FWHM of 136 nm) and EQE of  $\approx 0.1\%$ , at the luminance of  $1 \text{ cd m}^{-2}$ . Liu et al. fabricated CsCu<sub>2</sub>I<sub>3</sub> LEDs, where CsCu<sub>2</sub>I<sub>3</sub> powder was deposited with vacuum-based methods, demonstrating an EQE of 0.02% and luminance of  $10 \text{ cd m}^{-2}$ .<sup>[91]</sup> Ma et al. reported LEDs made from solution-processed CsCu<sub>2</sub>I<sub>3</sub> with emission peaking at 550 nm, reaching a maximum luminance of  $475 \text{ cd m}^{-2}$  and EQE of 0.17% and having an operational half-lifetime of 5.2 h at 25 °C.<sup>[92]</sup>

Broadly speaking, the above-mentioned lead-free materials are more thermally, operationally, and/or structurally stable than their halide perovskite analogues, but the broader emission spectrum, poorer charge transport properties, and/or higher defect-intolerance make them more challenging for applications that require tailored, controllable, and narrow emission spectra including in high-quality white light applications. Indeed, these broadband emitters may be more suitable in light-emission applications as scintillator detector or phosphor materials.

In contrast to blue, green, and orange lead-free LEDs, where Pb was substituted mainly by Sb, Cu, and Mn ions, for red and near-infrared LEDs the Pb replacement is achieved with Sn. Advantages of Sn-based emitters include their exploitation for color-pure red emission based on single halide structures, thus potentially circumventing the device instabilities of red Pb-based mixed halide perovskites owing to phase segregation.<sup>[93]</sup> Additionally, Sn-based LEDs can reach near-infrared emission wavelengths that are beyond the range of lead halide PeLEDs ( $>810 \text{ nm}$ ). Still, the facile oxidation of Sn<sup>2+</sup> to Sn<sup>4+</sup> in these Sn emitters remains problematic.<sup>[94]</sup> For red EL, a 2D (PEA)<sub>2</sub>SnI<sub>4</sub> emitter was used in an LED that reached a luminance of  $0.15 \text{ cd m}^{-2}$  and shows a peak emission at  $\approx 618 \text{ nm}$ .<sup>[95]</sup> Compared to a 0.01% PLQE for 3D MASnI<sub>3</sub>, the (PEA)<sub>2</sub>SnI<sub>4</sub> emitter showed higher PLQE values at 0.24%, which is attributed to the excitonic character of the 2D structure of (PEA)<sub>2</sub>SnI<sub>4</sub>. Moreover, the stability of (PEA)<sub>2</sub>SnI<sub>4</sub>, when stored in ambient air in the dark, was shown to be better compared to that of MASnI<sub>3</sub>, which is believed to be due to a slow-down of oxygen diffusion (and subsequent material degradation) into the perovskite film as a result of the presence of the larger organic cation in the structure. Liang et al. demonstrated reduced oxidation of Sn<sup>2+</sup> and improved film quality by using H<sub>3</sub>PO<sub>2</sub> as an additive to the (PEA)<sub>2</sub>SnI<sub>4</sub> precursor solution.<sup>[93]</sup> Their (PEA)<sub>2</sub>SnI<sub>4</sub> LEDs showed 0.3% peak EQE and  $70 \text{ cd m}^{-2}$  maximum luminance and emitted at 633 nm with FWHM of 24 nm. Using a similar strategy, Gao et al. enhanced the performance of (PEA)<sub>2</sub>SnI<sub>4</sub> LEDs to 0.72% EQE and  $132 \text{ cd m}^{-2}$  luminance by using 2,3-dihydroxynaphthalene-6-sulfonic acid sodium salt as an additive that facilitated the formation of a homogeneous (PEA)<sub>2</sub>SnI<sub>4</sub> thin film, passivated Sn<sup>2+</sup> dangling bonds, and reduced Sn<sup>2+</sup> oxidation.<sup>[96]</sup> The half-lifetime of the device under continuous operation at constant 3.4 V was 62 s. Also, Yuan et al. used the additive strategy to enhance the

performance of their  $(\text{PEA})_2\text{SnI}_4$  LEDs, which showed a 5% maximum EQE and an operating half-life of >15 h at initial luminance of  $20 \text{ cd m}^{-2}$ .<sup>[97]</sup> The use of valeric acid as an additive is proposed to protect  $\text{Sn}^{2+}$  from oxidation and results in a strong interaction of the acid with  $\text{Sn}^{2+}$ , which enhanced film morphology by reducing the crystallization rate of the perovskite precursors. Liao et al. used chlorobenzene as an antisolvent during the  $(\text{PEA})_2\text{SnI}_4$  spin-coating process, which led to an enhanced PLQE of the resulting  $(\text{PEA})_2\text{SnI}_4$  film.<sup>[98]</sup> Additionally, they used phenylhydrazine hydrochloride as a reducing agent to lessen oxidation of the film. Their  $(\text{PEA})_2\text{SnI}_4$  LEDs, fabricated using both the antisolvent and the reducing agent, showed peak EQE and luminance values of 0.52% and  $250 \text{ cd m}^{-2}$ , respectively. While the aforementioned approaches to enhance the EL performance of 2D tin-iodide-based emitters relied on the use of additives, Wang et al. replaced the PEA cation in  $(\text{PEA})_2\text{SnI}_4$  with TEA (TEA = 2-thiopheneethylammonium).<sup>[99]</sup> Their  $(\text{TEA})_2\text{SnI}_4$  LEDs showed EL at  $\approx 638 \text{ nm}$  (with FWHM of 28 nm), which is slightly redshifted compared with  $(\text{PEA})_2\text{SnI}_4$ . The authors attribute this redshift to the narrower bandgap of  $(\text{TEA})_2\text{SnI}_4$ , which results from a larger dielectric contrast  $\epsilon_w/\epsilon_b$  of  $(\text{TEA})_2\text{SnI}_4$  (where  $\epsilon_w$  and  $\epsilon_b$  are the dielectric constants of the inorganic layer and the organic barrier layer, respectively) compared to that of  $(\text{PEA})_2\text{SnI}_4$ . The LEDs based on  $(\text{TEA})_2\text{SnI}_4$  achieved a maximum luminance of  $322 \text{ cd m}^{-2}$  and had an EQE of 0.62%. Additionally, the  $(\text{TEA})_2\text{SnI}_4$  samples showed a higher exciton binding energy and lower trap state density than  $(\text{PEA})_2\text{SnI}_4$ . Apart from 2D Sn-based materials, 3D  $\text{CsSnBr}_3$  has also been explored for red-light EL.<sup>[100]</sup> The typical LED stack included (amongst others) a vacuum vapor-deposited  $\text{CsSnBr}_3$  thin film, sandwiched between two LiF layers, in an “insulator–perovskite–insulator” architecture, where injected electrons and holes tunnel through the respective LiF layers to recombine in the perovskite film. The  $\text{CsSnBr}_3$  LED with emission centered at 672 nm and a FWHM of  $\approx 54 \text{ nm}$  reached a peak EQE of  $\approx 0.34\%$  and luminance of  $\approx 172 \text{ cd m}^{-2}$ . The LED continuously operated for about 100 min under inert atmosphere and 6 V constant bias. Further, reports on red lead-free, perovskite-inspired LEDs aside Sn-based ones have remained scarce. However, Singh et al. fabricated LEDs based on  $\text{Cs}_3\text{Sb}_2\text{X}_9$  materials, where the broadly red-infrared-emitting  $\text{Cs}_3\text{Sb}_2\text{I}_9$  LED showed an EQE of  $\approx 10^{-8}$ , leaving ample room for improvement of device performance.<sup>[101]</sup>

For near-infrared perovskite-inspired LEDs, Lai et al. fabricated a  $\text{MASnI}_3$ -based LED, which emitted at 945 nm and had a peak EQE of 0.72% and a maximum radiance of  $3.4 \text{ W sr}^{-1} \text{ m}^{-2}$ .<sup>[102]</sup> If operated as an encapsulated device at constant 6 V applied voltage, the  $\text{MASnI}_3$  LED degraded rapidly and was nonluminescent after 6 min of operation. By increasing the bromine content in the  $\text{MASn}(\text{Br}_{1-x}\text{I}_x)_3$  structure, the EL of LEDs based on these materials could be tuned between 667 and 945 nm (for  $0.5 < x < 1$ ). However, a lack of luminescence in  $\text{MASn}(\text{Br}_{1-x}\text{I}_x)_3$  samples with higher bromine content ( $x < 0.5$ ) was attributed to higher structural disorder and prevented detection of EL from the corresponding higher Br-containing LEDs. Additionally, Hong et al. demonstrated a  $\text{CsSnI}_3$  LED with EL at 950 nm and maximum EQE and maximum radiance of 3.8% and  $40 \text{ W sr}^{-1} \text{ m}^{-2}$ , respectively.<sup>[94]</sup> Wang et al. reported LEDs based on  $(\text{PEAI})_x(\text{CsI})_y(\text{SnI}_2)_z$  multiple quantum well structures ( $x:y:z$

indicating the 3.5:5:4.5 molar ratios of  $\text{PEAI}:\text{CsI}:\text{SnI}_2$  precursors in solution), where the incorporation of bulky PEA aided the suppression of  $\text{Sn}^{2+}$  oxidation.<sup>[103]</sup> Their devices achieved a peak EQE of 3% and radiance of  $40 \text{ W sr}^{-1} \text{ m}^{-2}$  and showed an EL peak at 920 nm. Recently, solutions of  $\text{CsSnI}_3$  NCs were reported to photoluminesce at 938 nm with FWHM of 83 nm.<sup>[104]</sup> LEDs fabricated using these  $\text{CsSnI}_3$  NCs only showed a low maximum EQE of about 0.007%.

### 3. Challenges and Outlook

#### 3.1. Device Stability

While perovskite solar cells retain >95% of their efficiency after 1000 h under continuous solar illumination at  $60 \text{ }^\circ\text{C}$ ,<sup>[105]</sup> LEDs based on perovskite to date last less than 50 h under operation,<sup>[106–108]</sup> far behind state-of-the-art inorganic quantum dot LEDs and organic LEDs (up to a million hours).<sup>[109,110]</sup> The stability of PeLEDs is mainly compromised by moisture,<sup>[111–113]</sup> temperature,<sup>[114,115]</sup> photodegradation,<sup>[116–118]</sup> and bias-induced degradation.<sup>[119–121]</sup> Compared to the low electric field across the absorber layer in perovskite solar cells under operation, the high bias applied in PeLEDs based on relatively thinner active layers ( $\approx 500 \text{ nm}$  in solar cells to  $\approx 30 \text{ nm}$  in PeLEDs) causes severe ion migration in the devices, facilitating structural degradation, charge accumulation at interfaces, and corrosion of metal electrodes.<sup>[121,122]</sup> Methods applying protecting layers,<sup>[123,124]</sup> nonmetallic electrodes,<sup>[125,126]</sup> and MA-free perovskite<sup>[127,128]</sup> have shown promising improvements in device stability. However, the operational degradation of PeLEDs is not fully understood. A recent investigation reveals that PeLEDs under normal operation release gaseous degradation compounds which lead to local delamination of the cathodes and thus reduce the EL of devices.<sup>[114]</sup> On the other hand, irreversible accumulation of ions at an interface is observed in mixed halide PeLEDs, leading to charge-carrier injection barriers and nonradiative recombination.<sup>[129]</sup> The low formation energy of perovskite materials and the complex electrochemistry at the device interfaces remain big concerns for commercial light-emitting applications.<sup>[130,131]</sup>

It is widely known that halide perovskites suffer from photostabilities, showing both photobrightening and photodarkening effects.<sup>[132]</sup> These light-induced phenomena share a common underlying mechanism to some of the bias-induced instabilities found in PeLEDs, which are directly linked to the ionic character of the compounds and their migration processes triggered by electric fields. Therefore, it is crucial to understand how to achieve the ionic distributions at which peak operation occurs from time zero—and maintain it there. The photobrightening effect in perovskites excited under specific conditions of light and/or bias suggests there are achievable ionic distribution states which lead to very bright emission in PeLEDs. Through undesired chemical reactions with charge-injecting layers and bandgap shifts (color changes) or emission intensity variations in the perovskite layer, recent reports demonstrate a gamut of routes to freeze that transient behavior at its maximum.<sup>[133]</sup> This phenomenon is observed in EL leading to a “burn-in” or “luminance overshoot” under

operation attributed to ionic reorganization in perovskites that can be maintained for longer periods of operation with appropriate passivation.<sup>[129,134,135]</sup> Interestingly, some groups have taken advantage of this phenomenon to propose perovskite-based light-emitting electrochemical devices,<sup>[136]</sup> opening new avenues for these materials.<sup>[137]</sup> It remains to be seen if such approaches can stabilize operation over long periods, including mitigating against redox chemistry in these ionic systems in the presence of high densities of injected electrons under operating conditions—but such breakthroughs will be critical for realizing long-term stability.

However, achieving long-term stability of PeLEDs will require first minimizing a primary cause of performance degradation in devices—ion migration—by designing a perovskite emissive layer with higher structural resistance to electric stress. Compared to pure 3D or randomly assembled 2D/3D perovskites, pure 2D layered perovskite,<sup>[138]</sup> surface-2D/bulk-3D perovskite,<sup>[139]</sup> and perovskite-polymer composite films<sup>[61]</sup> exhibit more than tenfold operational time under constant bias. These results hint at routes to improve PeLED device stability. Introducing ion-blocking layers or using anticorrosive transport layers and electrodes can further extend the lifespan of PeLEDs.

### 3.2. Outcoupling Design

The demonstration of stable PeLEDs with EQEs surpassing 20% now motivates investigating routes based on light management to further boost the efficiencies. In general, one can describe PeLEDs as a succession of thin films, one stacked on top of the other. This multilayered nature, in which the thickness of the system is on the order of the wavelength of the emitted light, gives rise to strong interference phenomena. The understanding, modeling, and control of these effects are key to promote radiative recombination events within the active layer through localization of the electromagnetic field and maximizing light outcoupling. In principle, if we fix the materials comprising the device and thus the spectral dependence of their dielectric function (complex refractive index),<sup>[140–142]</sup> one can find the combination of layer thicknesses leading to optimal photon emission out of the system. This will come as a result of a convenient generation and propagation of photons across the device, which can be boosted through: i) antireflective phenomena that augment the number of outcoupled photons, ii) decreasing parasitic absorption due to light delocalization in non-active layers, iii) increasing radiative recombination events through light confinement in the perovskite film, and iv) formation of multilayer-like resonances at the emission wavelength. Given the strong overlap between absorption and emission of many of the perovskite emitter layers, photon recycling, in which emitted photons are reabsorbed by the emitter layer following by further emission events, needs to be accounted for.<sup>[143,144]</sup> Recent calculations show that under PeLED operating conditions each emitted photon may undertake up to ten recycling events before it is outcoupled from the device stack.<sup>[145]</sup> Such recycling events can increase the maximum attainable EQE by allowing further opportunities to outcouple in the forward direction, rather than being waveguided laterally out of the device as is the case in thin-film OLED structures.<sup>[146]</sup>

In addition to this noninvasive optical optimization of the PeLED, the thin-film nature of the system makes it ideal for its combination with structured materials showing beneficial features in the range of the PeLED emission spectrum. This will involve the inclusion of photonic, plasmonic, and dielectric nanostructures into the device—aspects that have been extensively studied for perovskite solar cells,<sup>[147,148]</sup> but remain mostly unexplored for PeLEDs.<sup>[149]</sup> This kind of optical design will be central to drive PeLEDs toward higher efficiency horizons.

### 3.3. Toward White Emission

Solid-state lighting is a major shift in artificial white lighting that has been driven by the development of highly efficient LEDs. For this reason, achieving efficient and cost-effective white emission is a holy grail for solid-state light emission applications based on perovskite materials, which represent an excellent opportunity for the realization of flexible panel lighting. However, blue PeLEDs, as a crucial component for white emission, still suffer from color instability and low efficiency. Blue-emitting perovskites are typically composed of mixed halide ions or quantum-confined low-dimensional structures to achieve suitable bandgaps. The color instability of PeLEDs based on mixed halide perovskite comes from phase segregation under the bias electrical field, where the blue EL peak shifts toward green at a working bias.<sup>[47,150]</sup> The relatively low PLQE of perovskite blue emitters arises from defect states close to the midgap which contribute to the recombination losses of the wider bandgap perovskite.<sup>[151]</sup> On the other hand, low-dimensional perovskites have achieved up to 80% PLQE with high color purity,<sup>[152]</sup> but carrier injection of these materials remains a problem. As typical low-dimensional perovskites are fabricated using long organic ligands,<sup>[43]</sup> optimizing surface ligands,<sup>[153–155]</sup> engineering interfaces,<sup>[71]</sup> and passivating surface defects<sup>[68,156,157]</sup> become crucial in improving charge injection for efficient blue PeLEDs. We believe that the combination of mixed-composition perovskites with a gradient of dimensionality (rather than labile halide composition) will lead to an optimum compromise between long-time operational stability and high luminescence yields through efficient charge carrier funneling. Additionally, the community is exploring a large family of alternative ionic materials that show promise for light-emission applications. For example, lead-free perovskite-inspired materials have recently shown promising blue light-emission characteristics.<sup>[158–162]</sup>

Another way to achieve white LEDs is through the use of wider gap 1D (Figure 7a–d)<sup>[163]</sup> or 2D-layered perovskites (Figure 7e,f),<sup>[164–166]</sup> which emit broad white light through self-trapped exciton recombination. However, as the emission is generated from a single source, tuning the white color of these LEDs is not as easy as in LEDs with multiple color sources, unless the emissive layer consists of different phases that coexist to produce tunable white EL. For instance, LEDs based on CsCu<sub>2</sub>I<sub>3</sub>@Cs<sub>3</sub>Cu<sub>2</sub>I<sub>5</sub> composites showed white-light emission originating from the combined EL of broadly yellow and broadly blue emitting CsCu<sub>2</sub>I<sub>3</sub> and Cs<sub>3</sub>Cu<sub>2</sub>I<sub>5</sub> phases, respectively.<sup>[167]</sup> Their devices achieved a maximum EQE of 0.15% and a luminance of 145 cd m<sup>-2</sup>. Recently, Chen et al. demonstrated white LEDs

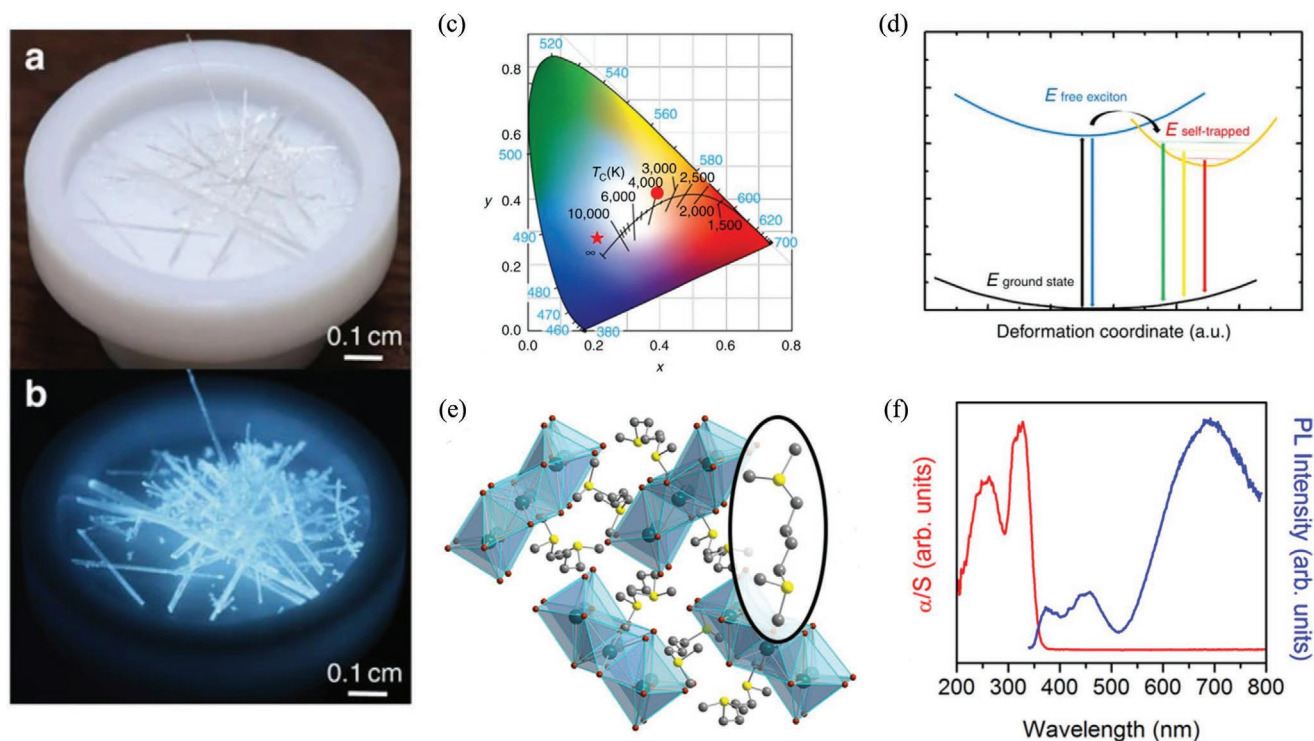


**Figure 7.** Image of bulk 1D  $C_4N_2H_{14}PbBr_4$  crystals under a) ambient light and b) UV light (365 nm). c) Commission Internationale de l'Eclairage chromaticity coordinates of the 1D perovskites (star) and the corrugated 2D perovskite (EDBE)  $PbBr_4$  (EDBE = 2,2'-(ethylenedioxy)bis(ethylammonium)). d) Configuration coordinate diagram for the coexisting of free and self-trapped excitons in 1D perovskites; the straight and curved arrows represent optical and relaxation transitions, respectively. Reproduced with permission.<sup>[163]</sup> Copyright 2017, Springer Nature. e) Crystal structure of 2D (1,4-bbdms)<sub>3</sub>Pb<sub>3</sub>Br<sub>12</sub> (1,4-bbdms = (CH<sub>3</sub>)<sub>2</sub>S(CH<sub>2</sub>)<sub>4</sub>(CH<sub>3</sub>)<sub>2</sub><sup>2+</sup>) perovskite. Inset: the 1,4-bbdms cation. Green, brown, yellow, and gray spheres represent Pb, Br, S, and C atoms, respectively. f) PL spectrum for powdered 2D (1,4-bbdms)<sub>3</sub>Pb<sub>3</sub>Br<sub>12</sub> perovskite. Reproduced with permission.<sup>[164]</sup> Copyright 2017, American Chemical Society.

based on a single perovskite layer of red-emitting  $\alpha$ -CsPbI<sub>3</sub> and white-emitting self-trapped  $\delta$ -CsPbI<sub>3</sub>, which showed an EQE of 6.5% and a peak luminance of 12 200 cd m<sup>-2</sup>.<sup>[168]</sup> However, tuning the white color of their LEDs requires careful control of the annealing process. A more practical way for tunable color temperature involves a combination of blue PeLEDs and orange-emitting perovskite<sup>[169,170]</sup> or nonperovskite phosphors.<sup>[171–173]</sup> On the other hand, blue LED chips covered with red and green perovskite color converters can also yield white emission, where perovskite quantum dots are embedded in organic silica shells to prevent contact with moisture and oxygen.<sup>[174–176]</sup> Digging further with the perovskite color converters, recent reports explore white emission from red, green, and blue (RGB) perovskite phosphors excited by UV background light sources, achieving high stability with continuous illumination at high power.<sup>[177–179]</sup> For commercial color displays such as television and phone screens, researchers use pixel-wise integration of independent RGB LEDs, where the color can be tuned by adjusting the emission intensity of each subpixel color source. Thus, advances of PeLEDs in each color are crucial to exploit this family of compounds and ensure their real-world application.

### 3.4. Perovskite-Inspired LEDs and Lasing

Inspired by the successful integration of 3D perovskites in highly efficient LEDs, other materials with similar structural

features are gaining increasing attentions including double perovskites,<sup>[167,168,180,181]</sup> hollow 3D perovskites,<sup>[182–185]</sup> 2D-layered perovskites,<sup>[164–166]</sup> and 1D<sup>[163,186]</sup> and 0D perovskites.<sup>[187–189]</sup> The properties of these materials need to be assessed on an individual material basis, which makes the generalization of material characteristics across certain classes of perovskite difficult. Principally, for the application of these materials in LEDs, the requirements to the material properties of the active LED material are set by the particular design and intended use of the LED. While lower-dimensional perovskites may have the additional advantage of large exciton binding energies, which increase radiative recombination and enhance PLQE,<sup>[190]</sup> many double perovskites overcome toxicity issues by replacing lead with less hazardous systems such as Bi<sup>[191–193]</sup> and Ag.<sup>[194,195]</sup> However, there are still important challenges to overcome to propose these materials for working devices including poor thin film morphology, indirect bandgaps, low emission yields, and large hole/electron-effective masses, which lead to low mobilities and poor charge transport.<sup>[196–198]</sup> Nonetheless, these challenges can be overcome with elaborate materials engineering. For example, fabrication of the efficient Bi-doped white-light-emitting bulk powder Cs<sub>2</sub>(Ag<sub>0.60</sub>Na<sub>0.40</sub>)InCl<sub>6</sub><sup>[199]</sup> into NCs,<sup>[200]</sup> band structure engineering via doping<sup>[201]</sup> or compositional tuning.<sup>[202–204]</sup>

Finally, halide perovskites and similarly inspired materials are sought as potential candidates for continuous-wave and electrically pumped solution-processed laser diodes. They

show sharp absorption onsets, low nonradiative recombination at carrier densities for population inversion, large gain cross section at the wavelength of emission, and excellent carrier mobilities; these properties make them suitable to support lasing.<sup>[205]</sup> In fact, optically driven lasing has been already well demonstrated in perovskites in which different strategies, such as Fabry-Perot cavities, whispering mode cavities, and random media, have been used to attain gain media of high quality.<sup>[206]</sup> However, the realization of electrically pumped perovskite lasers remains a challenge in the field, mainly because of both the relatively low Auger thresholds and the low material stability at the high temperatures that are induced in the system at the lasing regime.<sup>[207]</sup> Still, we foresee that the tunability of perovskites and their integrability with optically active elements may eventually allow for configurations in which electrically pumped lasing will be possible.

#### 4. Conclusion

Halide perovskites exhibit excellent properties such as highly efficient luminescence yields with narrow linewidths that, together with their versatile processability and bandgap tunability, make them good candidates for use in commercial light-emitting technologies. Although industry-ready operational stability and highly efficient blue PeLEDs are yet to be demonstrated, these materials have the potential to challenge the increasingly dominant market position of OLEDs for new generation displays and, in the longer term, that of the widely adopted traditional LEDs for white lighting. The processability of perovskite films to a broad range of passivation approaches enables devices with suppressed nonradiative recombination, pushing the emission yields in PeLEDs ever closer to the theoretical ceilings. Furthermore, their intrinsic nanostructured characteristics will allow them to be integrated within novel photonic and plasmonic designs which enable full control over color purity and directionality of light emission. These strategies could revolutionize solid-state lighting with a palette of possibilities for new light-emitting applications.

#### Acknowledgements

K.J. and A.A. acknowledge funding from the Royal Society. M.A. acknowledges the Marie Skłodowska-Curie actions (Grant Agreement No. 841386) under the European Union's Horizon 2020 research and innovation programme. The authors acknowledge the Engineering and Physical Sciences Research Council (EPSRC, EP/R023980/1) and the European Research Council (ERC) under the European Union's Horizon 2020 research and innovation program (HYPERION, Grant Agreement No. 756962). S.D.S. acknowledges funding from the Royal Society and Tata Group (UF150033).

#### Conflict of Interest

The authors declare no conflict of interest.

#### Keywords

3D perovskites, confined perovskites, device stability, light-emitting diodes, monochromatic emission, perovskite LEDs, white lighting

Received: December 11, 2020

Revised: January 27, 2021

Published online: March 3, 2021

- [1] M.-H. Chang, D. Das, P. V. Varde, M. Pecht, *Microelectron. Reliab.* **2012**, *52*, 762.
- [2] Z.-K. Tan, R. S. Moghaddam, M. L. Lai, P. Docampo, R. Higler, F. Deschler, M. Price, A. Sadhanala, L. M. Pazos, D. Credgington, F. Hanusch, T. Bein, H. J. Snaith, R. H. Friend, *Nat. Nanotechnol.* **2014**, *9*, 687.
- [3] Q. Lin, A. Armin, R. C. R. Nagiri, P. L. Burn, P. Meredith, *Nat. Photonics* **2015**, *9*, 106.
- [4] S. De Wolf, J. Holovsky, S.-J. Moon, P. Löper, B. Niesen, M. Ledinsky, F.-J. Haug, J.-H. Yum, C. Ballif, *J. Phys. Chem. Lett.* **2014**, *5*, 1035.
- [5] Q. Wang, Y. Shao, Q. Dong, Z. Xiao, Y. Yuan, J. Huang, *Energy Environ. Sci.* **2014**, *7*, 2359.
- [6] Q. Chen, H. Zhou, Z. Hong, S. Luo, H.-S. Duan, H.-H. Wang, Y. Liu, G. Li, Y. Yang, *J. Am. Chem. Soc.* **2014**, *136*, 622.
- [7] Z. Xiao, C. Bi, Y. Shao, Q. Dong, Q. Wang, Y. Yuan, C. Wang, Y. Gao, J. Huang, *Energy Environ. Sci.* **2014**, *7*, 2619.
- [8] G. E. Eperon, S. D. Stranks, C. Menelaou, M. B. Johnston, L. M. Herz, H. J. Snaith, *Energy Environ. Sci.* **2014**, *7*, 982.
- [9] W. Deng, X. Xu, X. Zhang, Y. Zhang, X. Jin, L. Wang, S.-T. Lee, J. Jie, *Adv. Funct. Mater.* **2016**, *26*, 4797.
- [10] J. Byun, H. Cho, C. Wolf, M. Jang, A. Sadhanala, R. H. Friend, H. Yang, T.-W. Lee, *Adv. Mater.* **2016**, *28*, 7515.
- [11] Q. Zhang, L. Chu, F. Zhou, W. Ji, G. Eda, *Adv. Mater.* **2018**, *30*, 1704055.
- [12] S. D. Stranks, V. M. Burlakov, T. Leijtens, J. M. Ball, A. Goriely, H. J. Snaith, *Phys. Rev. Appl.* **2014**, *2*, 034007.
- [13] I. L. Braly, D. W. deQuilettes, L. M. Pazos-Outón, S. Burke, M. E. Ziffer, D. S. Ginger, H. W. Hillhouse, *Nat. Photonics* **2018**, *12*, 355.
- [14] A. K. Jena, A. Kulkarni, T. Miyasaka, *Chem. Rev.* **2019**, *119*, 3036.
- [15] X. Li, F. Cao, D. Yu, J. Chen, Z. Sun, Y. Shen, Y. Zhu, L. Wang, Y. Wei, Y. Wu, H. Zeng, *Small* **2017**, *13*, 1603996.
- [16] J. Mao, W. E. I. Sha, H. Zhang, X. Ren, J. Zhuang, V. A. L. Roy, K. S. Wong, W. C. H. Choy, *Adv. Funct. Mater.* **2017**, *27*, 1606525.
- [17] Y. Wang, X. Li, J. Song, L. Xiao, H. Zeng, H. Sun, *Adv. Mater.* **2015**, *27*, 7101.
- [18] X. Hong, T. Ishihara, A. V. Nurmikko, *Solid State Commun.* **1992**, *84*, 657.
- [19] M. Era, S. Morimoto, T. Tsutsui, S. Saito, *Appl. Phys. Lett.* **1994**, *65*, 676.
- [20] T. Hattori, T. Taira, M. Era, T. Tsutsui, S. Saito, *Chem. Phys. Lett.* **1996**, *254*, 103.
- [21] K. Chondroudis, D. B. Mitzi, *Chem. Mater.* **1999**, *11*, 3028.
- [22] Y. Li, M. K. Fung, Z. Xie, S.-T. Lee, L.-S. Huang, J. Shi, *Adv. Mater.* **2002**, *14*, 1317.
- [23] J.-S. Kim, R. H. Friend, I. Grizzi, J. H. Burroughes, *Appl. Phys. Lett.* **2005**, *87*, 023506.
- [24] N. T. Kalyani, S. J. Dhoble, *Renewable Sustainable Energy Rev.* **2012**, *16*, 2696.
- [25] Y. Shirasaki, G. J. Supran, M. G. Bawendi, V. Bulović, *Nat. Photonics* **2013**, *7*, 13.

- [26] J. Wang, N. Wang, Y. Jin, J. Si, Z.-K. Tan, H. Du, L. Cheng, X. Dai, S. Bai, H. He, Z. Ye, M. L. Lai, R. H. Friend, W. Huang, *Adv. Mater.* **2015**, *27*, 2311.
- [27] G. Li, Z.-K. Tan, D. Di, M. L. Lai, L. Jiang, J. H.-W. Lim, R. H. Friend, N. C. Greenham, *Nano Lett.* **2015**, *15*, 2640.
- [28] E. T. Hoke, D. J. Slotcavage, E. R. Dohner, A. R. Bowring, H. I. Karunadasa, M. D. McGehee, *Chem. Sci.* **2015**, *6*, 613.
- [29] M. H. Futscher, J. M. Lee, L. McGovern, L. A. Muscarella, T. Wang, M. I. Haider, A. Fakhruddin, L. Schmidt-Mende, B. Ehrler, *Mater. Horiz.* **2019**, *6*, 1497.
- [30] M. Anaya, B. P. Rand, R. J. Holmes, D. Credgington, H. J. Bolink, R. H. Friend, J. Wang, N. C. Greenham, S. D. Stranks, *Nat. Photonics* **2019**, *13*, 818.
- [31] N. A. Luechinger, *SID Symp. Dig. Tech. Pap.* **2020**, *51*, 1178.
- [32] H.-L. Hsu, C.-P. Chen, J.-Y. Chang, Y.-Y. Yu, Y.-K. Shen, *Nanoscale* **2014**, *6*, 10281.
- [33] O. A. Jaramillo-Quintero, R. S. Sanchez, M. Rincon, I. Mora-Sero, *J. Phys. Chem. Lett.* **2015**, *6*, 1883.
- [34] H. Cho, S.-H. Jeong, M.-H. Park, Y.-H. Kim, C. Wolf, C.-L. Lee, J. H. Heo, A. Sadhanala, N. Myoung, S. Yoo, S. H. Im, R. H. Friend, T.-W. Lee, *Science* **2015**, *350*, 1222.
- [35] N. Yantara, S. Bhaukik, F. Yan, D. Sabba, H. A. Dewi, N. Mathews, P. P. Boix, H. V. Demir, S. Mhaisalkar, *J. Phys. Chem. Lett.* **2015**, *6*, 4360.
- [36] L. Zhang, X. Yang, Q. Jiang, P. Wang, Z. Yin, X. Zhang, H. Tan, Y. Yang, M. Wei, B. R. Sutherland, E. H. Sargent, J. You, *Nat. Commun.* **2017**, *8*, 15640.
- [37] M. V. Kovalenko, L. Protesescu, M. I. Bodnarchuk, *Science* **2017**, *358*, 745.
- [38] F. Zhang, H. Zhong, C. Chen, X.-G. Wu, X. Hu, H. Huang, J. Han, B. Zou, Y. Dong, *ACS Nano* **2015**, *9*, 4533.
- [39] L. C. Schmidt, A. Pertegás, S. González-Carrero, O. Malinkiewicz, S. Agouram, G. M. Espallargas, H. J. Bolink, R. E. Galian, J. Pérez-Prieto, *J. Am. Chem. Soc.* **2014**, *136*, 850.
- [40] H. Huang, F. Zhao, L. Liu, F. Zhang, X.-G. Wu, L. Shi, B. Zou, Q. Pei, H. Zhong, *ACS Appl. Mater. Interfaces* **2015**, *7*, 28128.
- [41] L. Protesescu, S. Yakunin, S. Kumar, J. Bär, F. Bertolotti, N. Masciocchi, A. Guagliardi, M. Grotevent, I. Shorubalko, M. I. Bodnarchuk, C.-J. Shih, M. V. Kovalenko, *ACS Nano* **2017**, *11*, 3119.
- [42] L. Protesescu, S. Yakunin, M. I. Bodnarchuk, F. Krieg, R. Caputo, C. H. Hendon, R. X. Yang, A. Walsh, M. V. Kovalenko, *Nano Lett.* **2015**, *15*, 3692.
- [43] J. Song, J. Li, X. Li, L. Xu, Y. Dong, H. Zeng, *Adv. Mater.* **2015**, *27*, 7162.
- [44] J. De Roo, M. Ibáñez, P. Geiregat, G. Nedelcu, W. Walravens, J. Maes, J. C. Martins, I. Van Driessche, M. V. Kovalenko, Z. Hens, *ACS Nano* **2016**, *10*, 2071.
- [45] J. Li, L. Xu, T. Wang, J. Song, J. Chen, J. Xue, Y. Dong, B. Cai, Q. Shan, B. Han, H. Zeng, *Adv. Mater.* **2017**, *29*, 1603885.
- [46] J. Pan, Y. Shang, J. Yin, M. De Bastiani, W. Peng, I. Dursun, L. Sinatra, A. M. El-Zohry, M. N. Hedhili, A.-H. Emwas, O. F. Mohammed, Z. Ning, O. M. Bakr, *J. Am. Chem. Soc.* **2018**, *140*, 562.
- [47] G. Li, F. W. R. Rivarola, N. J. L. K. Davis, S. Bai, T. C. Jellicoe, F. de la Peña, S. Hou, C. Ducati, F. Gao, R. H. Friend, N. C. Greenham, Z.-K. Tan, *Adv. Mater.* **2016**, *28*, 3528.
- [48] H.-C. Wang, W. Wang, A.-C. Tang, H.-Y. Tsai, Z. Bao, T. Ihara, N. Yarita, H. Tahara, Y. Kanemitsu, S. Chen, R.-S. Liu, *Angew. Chem.* **2017**, *129*, 13838.
- [49] M. Lu, X. Zhang, X. Bai, H. Wu, X. Shen, Y. Zhang, W. Zhang, W. Zheng, H. Song, W. W. Yu, A. L. Rogach, *ACS Energy Lett.* **2018**, *3*, 1571.
- [50] T. Chiba, Y. Hayashi, H. Ebe, K. Hoshi, J. Sato, S. Sato, Y.-J. Pu, S. Ohisa, J. Kido, *Nat. Photonics* **2018**, *12*, 681.
- [51] P. Vashishtha, J. E. Halpert, *Chem. Mater.* **2017**, *29*, 5965.
- [52] M. Yuan, L. N. Quan, R. Comin, G. Walters, R. Sabatini, O. Voznyy, S. Hoogland, Y. Zhao, E. M. Beauregard, P. Kanjanaboos, Z. Lu, D. H. Kim, E. H. Sargent, *Nat. Nanotechnol.* **2016**, *11*, 872.
- [53] N. Wang, L. Cheng, R. Ge, S. Zhang, Y. Miao, W. Zou, C. Yi, Y. Sun, Y. Cao, R. Yang, Y. Wei, Q. Guo, Y. Ke, M. Yu, Y. Jin, Y. Liu, Q. Ding, D. Di, L. Yang, G. Xing, H. Tian, C. Jin, F. Gao, R. H. Friend, J. Wang, W. Huang, *Nat. Photonics* **2016**, *10*, 699.
- [54] W. Zou, R. Li, S. Zhang, Y. Liu, N. Wang, Y. Cao, Y. Miao, M. Xu, Q. Guo, D. Di, L. Zhang, C. Yi, F. Gao, R. H. Friend, J. Wang, W. Huang, *Nat. Commun.* **2018**, *9*, 608.
- [55] L. N. Quan, Y. Zhao, F. P. G. de Arquer, R. Sabatini, G. Walters, O. Voznyy, R. Comin, Y. Li, J. Z. Fan, H. Tan, J. Pan, M. Yuan, O. M. Bakr, Z. Lu, D. H. Kim, E. H. Sargent, *Nano Lett.* **2017**, *17*, 3701.
- [56] M. Ban, Y. Zou, J. P. H. Rivett, Y. Yang, T. H. Thomas, Y. Tan, T. Song, X. Gao, D. Credgington, F. Deschler, H. Sirringhaus, B. Sun, *Nat. Commun.* **2018**, *9*, 3892.
- [57] X. Yang, X. Zhang, J. Deng, Z. Chu, Q. Jiang, J. Meng, P. Wang, L. Zhang, Z. Yin, J. You, *Nat. Commun.* **2018**, *9*, 570.
- [58] J. Li, S. G. R. Bade, X. Shan, Z. Yu, *Adv. Mater.* **2015**, *27*, 5196.
- [59] Y. Ling, Y. Tian, X. Wang, J. C. Wang, J. M. Knox, F. Perez-Orive, Y. Du, L. Tan, K. Hanson, B. Ma, H. Gao, *Adv. Mater.* **2016**, *28*, 8983.
- [60] Y. Cao, N. Wang, H. Tian, J. Guo, Y. Wei, H. Chen, Y. Miao, W. Zou, K. Pan, Y. He, H. Cao, Y. Ke, M. Xu, Y. Wang, M. Yang, K. Du, Z. Fu, D. Kong, D. Dai, Y. Jin, G. Li, H. Li, Q. Peng, J. Wang, W. Huang, *Nature* **2018**, *562*, 249.
- [61] B. Zhao, S. Bai, V. Kim, R. Lamboll, R. Shivanna, F. Auras, J. M. Richter, L. Yang, L. Dai, M. Alsari, X.-J. She, L. Liang, J. Zhang, S. Lilliu, P. Gao, H. J. Snaith, J. Wang, N. C. Greenham, R. H. Friend, D. Di, *Nat. Photonics* **2018**, *12*, 783.
- [62] K. Lin, J. Xing, L. N. Quan, F. P. G. de Arquer, X. Gong, J. Lu, L. Xie, W. Zhao, D. Zhang, C. Yan, W. Li, X. Liu, Y. Lu, J. Kirman, E. H. Sargent, Q. Xiong, Z. Wei, *Nature* **2018**, *562*, 245.
- [63] L. Song, X. Guo, Y. Hu, Y. Lv, J. Lin, Z. Liu, Y. Fan, X. Liu, *J. Phys. Chem. Lett.* **2017**, *8*, 4148.
- [64] W. Xu, Q. Hu, S. Bai, C. Bao, Y. Miao, Z. Yuan, T. Borzda, A. J. Barker, E. Tyukalova, Z. Hu, M. Kawecki, H. Wang, Z. Yan, X. Liu, X. Shi, K. Uvdal, M. Fahlman, W. Zhang, M. Duchamp, J.-M. Liu, A. Petrozza, J. Wang, L.-M. Liu, W. Huang, F. Gao, *Nat. Photonics* **2019**, *13*, 418.
- [65] A. Sadhanala, S. Ahmad, B. Zhao, N. Giesbrecht, P. M. Pearce, F. Deschler, R. L. Z. Hoye, K. C. Gödel, T. Bein, P. Docampo, S. E. Dutton, M. F. L. De Volder, R. H. Friend, *Nano Lett.* **2015**, *15*, 6095.
- [66] N. K. Kumawat, A. Dey, A. Kumar, S. P. Gopinathan, K. L. Narasimhan, D. Kabra, *ACS Appl. Mater. Interfaces* **2015**, *7*, 13119.
- [67] H. P. Kim, J. Kim, B. S. Kim, H.-M. Kim, J. Kim, A. R. M. Yusoff, J. Jang, M. K. Nazeeruddin, *Adv. Opt. Mater.* **2017**, *5*, 1600920.
- [68] J. Pan, L. N. Quan, Y. Zhao, W. Peng, B. Murali, S. P. Sarmah, M. Yuan, L. Sinatra, N. M. Alyami, J. Liu, E. Yassitepe, Z. Yang, O. Voznyy, R. Comin, M. N. Hedhili, O. F. Mohammed, Z. H. Lu, D. H. Kim, E. H. Sargent, O. M. Bakr, *Adv. Mater.* **2016**, *28*, 8718.
- [69] Q. A. Akkerman, S. G. Motti, A. R. S. Kandada, E. Mosconi, V. D'Innocenzo, G. Bertoni, S. Marras, B. A. Kamino, L. Miranda, F. De Angelis, A. Petrozza, M. Prato, L. Manna, *J. Am. Chem. Soc.* **2016**, *138*, 1010.
- [70] Y. Wu, C. Wei, X. Li, Y. Li, S. Qiu, W. Shen, B. Cai, Z. Sun, D. Yang, Z. Deng, H. Zeng, *ACS Energy Lett.* **2018**, *3*, 2030.
- [71] R. L. Z. Hoye, M.-L. Lai, M. Anaya, Y. Tong, K. Gałkowski, T. Doherty, W. Li, T. N. Huq, S. Mackowski, L. Polavarapu, J. Feldmann, J. L. MacManus-Driscoll, R. H. Friend, A. S. Urban, S. D. Stranks, *ACS Energy Lett.* **2019**, *4*, 1181.



- [72] S. Kumar, J. Jagielski, S. Yakunin, P. Rice, Y.-C. Chiu, M. Wang, G. Nedelcu, Y. Kim, S. Lin, E. J. G. Santos, M. V. Kovalenko, C.-J. Shih, *ACS Nano* **2016**, *10*, 9720.
- [73] D. Liang, Y. Peng, Y. Fu, M. J. Shearer, J. Zhang, J. Zhai, Y. Zhang, R. J. Hamers, T. L. Andrew, S. Jin, *ACS Nano* **2016**, *10*, 6897.
- [74] J. Xing, Y. Zhao, M. Askerka, L. N. Quan, X. Gong, W. Zhao, J. Zhao, H. Tan, G. Long, L. Gao, Z. Yang, O. Voznyy, J. Tang, Z.-H. Lu, Q. Xiong, E. H. Sargent, *Nat. Commun.* **2018**, *9*, 3541.
- [75] Q. Wang, J. Ren, X.-F. Peng, X.-X. Ji, X.-H. Yang, *ACS Appl. Mater. Interfaces* **2017**, *9*, 29901.
- [76] Y.-K. Wang, D. Ma, F. Yuan, K. Singh, J. M. Pina, A. Johnston, Y. Dong, C. Zhou, B. Chen, B. Sun, H. Ebe, J. Fan, M.-J. Sun, Y. Gao, Z.-H. Lu, O. Voznyy, L.-S. Liao, E. H. Sargent, *Nat. Commun.* **2020**, *11*, 3674.
- [77] C. Wang, D. Han, J. Wang, Y. Yang, X. Liu, S. Huang, X. Zhang, S. Chang, K. Wu, H. Zhong, *Nat. Commun.* **2020**, *11*, 6428.
- [78] Y. Liu, J. Cui, K. Du, H. Tian, Z. He, Q. Zhou, Z. Yang, Y. Deng, D. Chen, X. Zuo, Y. Ren, L. Wang, H. Zhu, B. Zhao, D. Di, J. Wang, R. H. Friend, Y. Jin, *Nat. Photonics* **2019**, *13*, 760.
- [79] Z. Chu, Y. Zhao, F. Ma, C.-X. Zhang, H. Deng, F. Gao, Q. Ye, J. Meng, Z. Yin, X. Zhang, J. You, *Nat. Commun.* **2020**, *11*, 4165.
- [80] Y. Dong, Y.-K. Wang, F. Yuan, A. Johnston, Y. Liu, D. Ma, M.-J. Choi, B. Chen, M. Chekini, S.-W. Baek, L. K. Sagar, J. Fan, Y. Hou, M. Wu, S. Lee, B. Sun, S. Hoogland, R. Quintero-Bermudez, H. Ebe, P. Todorovic, F. Dinic, P. Li, H. T. Kung, M. I. Saidaminov, E. Kumacheva, E. Spiecker, L.-S. Liao, O. Voznyy, Z.-H. Lu, E. H. Sargent, *Nat. Nanotechnol.* **2020**, *15*, 668.
- [81] M. Karlsson, Z. Yi, S. Reichert, X. Luo, W. Lin, Z. Zhang, C. Bao, R. Zhang, S. Bai, G. Zheng, P. Teng, L. Duan, Y. Lu, K. Zheng, T. Pullerits, C. Deibel, W. Xu, R. Friend, F. Gao, *Nat. Commun.* **2021**, *12*, 361.
- [82] Z. Ma, Z. Shi, D. Yang, F. Zhang, S. Li, L. Wang, D. Wu, Y. Zhang, G. Na, L. Zhang, X. Li, Y. Zhang, C. Shan, *ACS Energy Lett.* **2020**, *5*, 385.
- [83] T. Jun, K. Sim, S. Iimura, M. Sasase, H. Kamioka, J. Kim, H. Hosono, *Adv. Mater.* **2018**, *30*, 1804547.
- [84] H. Chen, J. M. Pina, F. Yuan, A. Johnston, D. Ma, B. Chen, Z. Li, A. Dumont, X. Li, Y. Liu, S. Hoogland, Z. Zajacz, Z. Lu, E. H. Sargent, *J. Phys. Chem. Lett.* **2020**, *11*, 4326.
- [85] L. Wang, Z. Shi, Z. Ma, D. Yang, F. Zhang, X. Ji, M. Wang, X. Chen, G. Na, S. Chen, D. Wu, Y. Zhang, X. Li, L. Zhang, C. Shan, *Nano Lett.* **2020**, *20*, 3568.
- [86] I. Pelant, J. Valenta, *Luminescence Spectroscopy of Semiconductors*, Oxford University Press, Oxford, UK **2012**.
- [87] S. Li, J. Luo, J. Liu, J. Tang, *J. Phys. Chem. Lett.* **2019**, *10*, 1999.
- [88] L.-J. Xu, C.-Z. Sun, H. Xiao, Y. Wu, Z.-N. Chen, *Adv. Mater.* **2017**, *29*, 1605739.
- [89] X. Zhang, C. Wang, Y. Zhang, X. Zhang, S. Wang, M. Lu, H. Cui, S. V. Kershaw, W. W. Yu, A. L. Rogach, *ACS Energy Lett.* **2019**, *4*, 242.
- [90] R. Roccanova, A. Yangui, G. Seo, T. D. Creason, Y. Wu, D. Y. Kim, M.-H. Du, B. Saparov, *ACS Mater. Lett.* **2019**, *1*, 459.
- [91] N. Liu, X. Zhao, M. Xia, G. Niu, Q. Guo, L. Gao, J. Tang, *J. Semicond.* **2020**, *41*, 052204.
- [92] Z. Ma, Z. Shi, C. Qin, M. Cui, D. Yang, X. Wang, L. Wang, X. Ji, X. Chen, J. Sun, D. Wu, Y. Zhang, X. J. Li, L. Zhang, C. Shan, *ACS Nano* **2020**, *14*, 4475.
- [93] H. Liang, F. Yuan, A. Johnston, C. Gao, H. Choubisa, Y. Gao, Y.-K. Wang, L. K. Sagar, B. Sun, P. Li, G. Bappi, B. Chen, J. Li, Y. Wang, Y. Dong, D. Ma, Y. Gao, Y. Liu, M. Yuan, M. I. Saidaminov, S. Hoogland, Z.-H. Lu, E. H. Sargent, *Adv. Sci.* **2020**, *7*, 1903213.
- [94] W.-L. Hong, Y.-C. Huang, C.-Y. Chang, Z.-C. Zhang, H.-R. Tsai, N.-Y. Chang, Y.-C. Chao, *Adv. Mater.* **2016**, *28*, 8029.
- [95] L. Lanzetta, J. M. Marin-Beloqui, I. Sanchez-Molina, D. Ding, S. A. Haque, *ACS Energy Lett.* **2017**, *2*, 1662.
- [96] C. Gao, Y. Jiang, C. Sun, J. Han, T. He, Y. Huang, K. Yao, M. Han, X. Wang, Y. Wang, Y. Gao, Y. Liu, M. Yuan, H. Liang, *ACS Photonics* **2020**, *7*, 1915.
- [97] F. Yuan, X. Zheng, A. Johnston, Y.-K. Wang, C. Zhou, Y. Dong, B. Chen, H. Chen, J. Z. Fan, G. Sharma, P. Li, Y. Gao, O. Voznyy, H.-T. Kung, Z.-H. Lu, O. M. Bakr, E. H. Sargent, *Sci. Adv.* **2020**, *6*, eabb0253.
- [98] Y. Liao, Y. Shang, Q. Wei, H. Wang, Z. Ning, *J. Phys. D: Appl. Phys.* **2020**, *53*, 414005.
- [99] Z. Wang, F. Wang, B. Zhao, S. Qu, T. Hayat, A. Alsaedi, L. Sui, K. Yuan, J. Zhang, Z. Wei, Z. Tan, *J. Phys. Chem. Lett.* **2020**, *11*, 1120.
- [100] F. Yuan, J. Xi, H. Dong, K. Xi, W. Zhang, C. Ran, B. Jiao, X. Hou, A. K.-Y. Jen, Z. Wu, *Phys. Status Solidi RRL* **2018**, *12*, 1800090.
- [101] A. Singh, N.-C. Chiu, K. M. Boopathi, Y.-J. Lu, A. Mohapatra, G. Li, Y.-F. Chen, T.-F. Guo, C.-W. Chu, *ACS Appl. Mater. Interfaces* **2019**, *11*, 35088.
- [102] M. L. Lai, T. Y. S. Tay, A. Sadhanala, S. E. Dutton, G. Li, R. H. Friend, Z.-K. Tan, *J. Phys. Chem. Lett.* **2016**, *7*, 2653.
- [103] Y. Wang, R. Zou, J. Chang, Z. Fu, Y. Cao, L. Zhang, Y. Wei, D. Kong, W. Zou, K. Wen, N. Fan, N. Wang, W. Huang, J. Wang, *J. Phys. Chem. Lett.* **2019**, *10*, 453.
- [104] K. P. O. Mahesh, C.-Y. Chang, W.-L. Hong, T.-H. Wen, P.-H. Lo, H.-Z. Chiu, C.-L. Hsu, S.-F. Horng, Y.-C. Chao, *RSC Adv.* **2020**, *10*, 37161.
- [105] N. Arora, M. I. Dar, A. Hinderhofer, N. Pellet, F. Schreiber, S. M. Zakeeruddin, M. Grätzel, *Science* **2017**, *358*, 768.
- [106] Y. Miao, Y. Ke, N. Wang, W. Zou, M. Xu, Y. Cao, Y. Sun, R. Yang, Y. Wang, Y. Tong, W. Xu, L. Zhang, R. Li, J. Li, H. He, Y. Jin, F. Gao, W. Huang, J. Wang, *Nat. Commun.* **2019**, *10*, 3624.
- [107] L. Zhao, K. M. Lee, K. Roh, S. U. Z. Khan, B. P. Rand, *Adv. Mater.* **2019**, *31*, 1805836.
- [108] R. F. Service, *Science* **2019**, *364*, 918.
- [109] Y.-H. Won, O. Cho, T. Kim, D.-Y. Chung, T. Kim, H. Chung, H. Jang, J. Lee, D. Kim, E. Jang, *Nature* **2019**, *575*, 634.
- [110] M. Hack, M. S. Weaver, J. J. Brown, W.-Y. So, C. H. Brown, *US* **10,229,956**, **2019**.
- [111] D. Di Girolamo, M. I. Dar, D. Dini, L. Gontrani, R. Caminiti, A. Mattoni, M. Graetzel, S. Meloni, *J. Mater. Chem. A* **2019**, *7*, 12292.
- [112] W. Deng, X. Jin, Y. Lv, X. Zhang, X. Zhang, J. Jie, *Adv. Funct. Mater.* **2019**, *29*, 1903861.
- [113] S. Chen, A. Solanki, J. Pan, T. C. Sum, *Coatings* **2019**, *9*, 535.
- [114] V. Prakasam, D. Tordera, H. J. Bolink, G. Gelinck, *Adv. Opt. Mater.* **2019**, *7*, 1900902.
- [115] B. Conings, J. Drijkoningen, N. Gauquelin, A. Babayigit, J. D'Haen, L. D'Olieslaeger, A. Ethirajan, J. Verbeeck, J. Manca, E. Mosconi, F. De Angelis, H.-G. Boyen, *Adv. Energy Mater.* **2015**, *5*, 1500477.
- [116] H. Cho, Y.-H. Kim, C. Wolf, H.-D. Lee, T.-W. Lee, *Adv. Mater.* **2018**, *30*, 1704587.
- [117] J. Li, L. Wang, X. Yuan, B. Bo, H. Li, J. Zhao, X. Gao, *Mater. Res. Bull.* **2018**, *102*, 86.
- [118] R.-P. Xu, Y.-Q. Li, T.-Y. Jin, Y.-Q. Liu, Q.-Y. Bao, C. O'Carroll, J.-X. Tang, *ACS Appl. Mater. Interfaces* **2018**, *10*, 6737.
- [119] B. Xu, W. Wang, X. Zhang, H. Liu, Y. Zhang, G. Mei, S. Chen, K. Wang, L. Wang, X. W. Sun, *Sci. Rep.* **2018**, *8*, 15799.
- [120] H. Lee, D. Ko, C. Lee, *ACS Appl. Mater. Interfaces* **2019**, *11*, 11667.
- [121] Q. Dong, L. Lei, J. Mendes, F. So, *J. Phys. Mater.* **2020**, *3*, 012002.
- [122] G. Li, K. Chen, Y. Cui, Y. Zhang, Y. Tian, B. Tian, Y. Hao, Y. Wu, H. Zhang, *Adv. Opt. Mater.* **2020**, *8*, 1902012.
- [123] F. Bella, G. Griffini, J.-P. Correa-Baena, G. Saracco, M. Grätzel, A. Hagfeldt, S. Turri, C. Gerbaldi, *Science* **2016**, *354*, 203.
- [124] K. A. Bush, A. F. Palmstrom, Z. J. Yu, M. Boccard, R. Cheacharoen, J. P. Mailoa, D. P. McMeekin, R. L. Z. Hoye, C. D. Bailie, T. Leijtens, I. M. Peters, M. C. Minichetti, N. Rolston, R. Prasanna, S. Sofia,

- D. Harwood, W. Ma, F. Moghadam, H. J. Snaith, T. Buonassisi, Z. C. Holman, S. F. Bent, M. D. McGehee, *Nat. Energy* **2017**, *2*, 17009.
- [125] C. C. Boyd, R. Cheacharoen, K. A. Bush, R. Prasanna, T. Leijtens, M. D. McGehee, *ACS Energy Lett.* **2018**, *3*, 1772.
- [126] G. Grancini, C. Roldán-Carmona, I. Zimmermann, E. Mosconi, X. Lee, D. Martineau, S. Narbey, F. Oswald, F. De Angelis, M. Grätzel, M. K. Nazeeruddin, *Nat. Commun.* **2017**, *8*, 15684.
- [127] D. P. McMeekin, G. Sadoughi, W. Rehman, G. E. Eperon, M. Saliba, M. T. Hörlantner, A. Haghighirad, N. Sakai, L. Korte, B. Rech, M. B. Johnston, L. M. Herz, H. J. Snaith, *Science* **2016**, *351*, 151.
- [128] Z. Li, M. Yang, J.-S. Park, S.-H. Wei, J. J. Berry, K. Zhu, *Chem. Mater.* **2016**, *28*, 284.
- [129] Z. Andaji-Garmaroudi, M. Abdi-Jalebi, F. U. Kosasih, T. Doherty, S. Macpherson, A. R. Bowman, G. J. Man, U. B. Cappel, H. Rensmo, C. Ducati, R. H. Friend, S. D. Stranks, *Adv. Energy Mater.* **2020**, *10*, 2002676.
- [130] C. C. Boyd, R. Cheacharoen, T. Leijtens, M. D. McGehee, *Chem. Rev.* **2019**, *119*, 3418.
- [131] D. Bryant, N. Aristidou, S. Pont, I. Sanchez-Molina, T. Chotchuna ngatchaval, S. Wheeler, J. R. Durrant, S. A. Haque, *Energy Environ. Sci.* **2016**, *9*, 1655.
- [132] R. Brenes, D. Guo, A. Oshero, N. K. Noel, C. Eames, E. M. Hutter, S. K. Pathak, F. Niroui, R. H. Friend, M. S. Islam, H. J. Snaith, V. Bulović, T. J. Savenije, S. D. Stranks, *Joule* **2017**, *1*, 155.
- [133] Z. Andaji-Garmaroudi, M. Anaya, A. J. Pearson, S. D. Stranks, *Adv. Energy Mater.* **2020**, *10*, 1903109.
- [134] H. Kim, J. S. Kim, J.-M. Heo, M. Pei, I.-H. Park, Z. Liu, H. J. Yun, M.-H. Park, S.-H. Jeong, Y.-H. Kim, J.-W. Park, E. Oveisi, S. Nagane, A. Sadhanala, L. Zhang, J. J. Kweon, S. K. Lee, H. Yang, H. M. Jang, R. H. Friend, K. P. Loh, M. K. Nazeeruddin, N.-G. Park, T.-W. Lee, *Nat. Commun.* **2020**, *11*, 3378.
- [135] N. Li, L. Song, Y. Jia, Y. Dong, F. Xie, L. Wang, S. Tao, N. Zhao, *Adv. Mater.* **2020**, *32*, 1907786.
- [136] M. F. Aygüler, M. D. Weber, B. M. D. Puscher, D. D. Medina, P. Docampo, R. D. Costa, *J. Phys. Chem. C* **2015**, *119*, 12047.
- [137] A. Walsh, S. D. Stranks, *ACS Energy Lett.* **2018**, *3*, 1983.
- [138] H. Tsai, W. Nie, J.-C. Blancon, C. C. Stoumpos, C. M. M. Soe, J. Yoo, J. Crochet, S. Tretiak, J. Even, A. Sadhanala, G. Azzellino, R. Brenes, P. M. Ajayan, V. Bulović, S. D. Stranks, R. H. Friend, M. G. Kanatzidis, A. D. Mohite, *Adv. Mater.* **2018**, *30*, 1704217.
- [139] T.-H. Han, J.-W. Lee, Y. J. Choi, C. Choi, S. Tan, S.-J. Lee, Y. Zhao, Y. Huang, D. Kim, Y. Yang, *Adv. Mater.* **2020**, *32*, 1905674.
- [140] M. Anaya, G. Lozano, M. E. Calvo, W. Zhang, M. B. Johnston, H. J. Snaith, H. Míguez, *J. Phys. Chem. Lett.* **2015**, *6*, 48.
- [141] M. Anaya, J. P. Correa-Baena, G. Lozano, M. Saliba, P. Anguita, B. Roose, A. Abate, U. Steiner, M. Grätzel, M. E. Calvo, A. Hagfeldt, H. Míguez, *J. Mater. Chem. A* **2016**, *4*, 11214.
- [142] M. E. Calvo, *J. Mater. Chem. A* **2017**, *5*, 20561.
- [143] L. M. Pazos-Outón, M. Szumilo, R. Lamboll, J. M. Richter, M. Crespo-Quesada, M. Abdi-Jalebi, H. J. Beeson, M. Vručinić, M. Alsari, H. J. Snaith, B. Ehrler, R. H. Friend, F. Deschler, *Science* **2016**, *351*, 1430.
- [144] C. Cho, B. Zhao, G. D. Tainter, J.-Y. Lee, R. H. Friend, D. Di, F. Deschler, N. C. Greenham, *Nat. Commun.* **2020**, *11*, 611.
- [145] A. R. Bowman, M. Anaya, N. C. Greenham, S. D. Stranks, *Phys. Rev. Lett.* **2020**, *125*, 067401.
- [146] S. D. Stranks, R. L. Z. Hoye, D. Di, R. H. Friend, F. Deschler, *Adv. Mater.* **2019**, *31*, 1803336.
- [147] Y. Zhang, C.-K. Lim, Z. Dai, G. Yu, J. W. Haus, H. Zhang, P. N. Prasad, *Phys. Rep.* **2019**, *795*, 1.
- [148] H. Zhang, J. Toudert, *Sci. Technol. Adv. Mater.* **2018**, *19*, 411.
- [149] Q. Zhang, M. M. Tavakoli, L. Gu, D. Zhang, L. Tang, Y. Gao, J. Guo, Y. Lin, S.-F. Leung, S. Poddar, Y. Fu, Z. Fan, *Nat. Commun.* **2019**, *10*, 727.
- [150] M. K. Gangishetty, S. Hou, Q. Quan, D. N. Congreve, *Adv. Mater.* **2018**, *30*, 1706226.
- [151] C. M. Sutter-Fella, D. W. Miller, Q. P. Ngo, E. T. Roe, F. M. Toma, I. D. Sharp, M. C. Lonergan, A. Javey, *ACS Energy Lett.* **2017**, *2*, 709.
- [152] X. Gong, O. Voznyy, A. Jain, W. Liu, R. Sabatini, Z. Piontkowski, G. Walters, G. Bappi, S. Nokhrin, O. Bushuyev, M. Yuan, R. Comin, D. McCamant, S. O. Kelley, E. H. Sargent, *Nat. Mater.* **2018**, *17*, 550.
- [153] A. Pan, B. He, X. Fan, Z. Liu, J. J. Urban, A. P. Alivisatos, L. He, Y. Liu, *ACS Nano* **2016**, *10*, 7943.
- [154] Q. Shan, J. Li, J. Song, Y. Zou, L. Xu, J. Xue, Y. Dong, C. Huo, J. Chen, B. Han, H. Zeng, *J. Mater. Chem. C* **2017**, *5*, 4565.
- [155] T. Chiba, K. Hoshi, Y.-J. Pu, Y. Takeda, Y. Hayashi, S. Ohisa, S. Kawata, J. Kido, *ACS Appl. Mater. Interfaces* **2017**, *9*, 18054.
- [156] A. Kirakosyan, S. Yun, S.-G. Yoon, J. Choi, *Nanoscale* **2018**, *10*, 1885.
- [157] D. Parobek, B. J. Roman, Y. Dong, H. Jin, E. Lee, M. Sheldon, D. H. Son, *Nano Lett.* **2016**, *16*, 7376.
- [158] J. Zhang, Y. Yang, H. Deng, U. Farooq, X. Yang, J. Khan, J. Tang, H. Song, *ACS Nano* **2017**, *11*, 9294.
- [159] M. Leng, Y. Yang, K. Zeng, Z. Chen, Z. Tan, S. Li, J. Li, B. Xu, D. Li, M. P. Hautzinger, Y. Fu, T. Zhai, L. Xu, G. Niu, S. Jin, J. Tang, *Adv. Funct. Mater.* **2018**, *28*, 1704446.
- [160] J. Huang, T. Lei, M. Siron, Y. Zhang, S. Yu, F. Seeler, A. Dehestani, L. N. Quan, K. Schierle-Arndt, P. Yang, *Nano Lett.* **2020**, *20*, 3734.
- [161] J.-L. Xie, Z.-Q. Huang, B. Wang, W.-J. Chen, W.-X. Lu, X. Liu, J.-L. Song, *Nanoscale* **2019**, *11*, 6719.
- [162] L. Lian, M. Zheng, P. Zhang, Z. Zheng, K. Du, W. Lei, J. Gao, G. Niu, D. Zhang, T. Zhai, S. Jin, J. Tang, X. Zhang, J. Zhang, *Chem. Mater.* **2020**, *32*, 3462.
- [163] Z. Yuan, C. Zhou, Y. Tian, Y. Shu, J. Messier, J. C. Wang, L. J. van de Burgt, K. Kountouriotis, Y. Xin, E. Holt, K. Schanze, R. Clark, T. Siegrist, B. Ma, *Nat. Commun.* **2017**, *8*, 14051.
- [164] M. D. Smith, B. L. Watson, R. H. Dauskardt, H. I. Karunadasa, *Chem. Mater.* **2017**, *29*, 7083.
- [165] E. R. Dohner, E. T. Hoke, H. I. Karunadasa, *J. Am. Chem. Soc.* **2014**, *136*, 1718.
- [166] L. Mao, Y. Wu, C. C. Stoumpos, B. Traore, C. Katan, J. Even, M. R. Wasielewski, M. G. Kanatzidis, *J. Am. Chem. Soc.* **2017**, *139*, 11956.
- [167] Z. Ma, Z. Shi, D. Yang, Y. Li, F. Zhang, L. Wang, X. Chen, D. Wu, Y. Tian, Y. Zhang, L. Zhang, X. Li, C. Shan, *Adv. Mater.* **2021**, *33*, 2001367.
- [168] J. Chen, J. Wang, X. Xu, J. Li, J. Song, S. Lan, S. Liu, B. Cai, B. Han, J. T. Precht, D. Ginger, H. Zeng, *Nat. Photonics* **2020**, <https://doi.org/10.1038/s41566-020-00743-1>.
- [169] Y. Ke, B. Zhao, K. Ding, Y. Wang, S. Shu, B. Deng, G. Wang, R. Yu, *J. Lumin.* **2020**, *221*, 116997.
- [170] Q. Liu, L. Wang, W. Huang, X. Li, M. Yu, Q. Zhang, *Ceram. Int.* **2018**, *44*, 1662.
- [171] E.-P. Yao, Z. Yang, L. Meng, P. Sun, S. Dong, Y. Yang, Y. Yang, *Adv. Mater.* **2017**, *29*, 1606859.
- [172] L.-C. Chen, Z.-L. Tseng, W.-W. Chang, Y. W. Lin, *Ceram. Int.* **2018**, *44*, 3868.
- [173] M. Zhang, M. Wang, Z. Yang, J. Li, H. Qiu, *J. Alloys Compd.* **2018**, *748*, 537.
- [174] C. Sun, Y. Zhang, C. Ruan, C. Yin, X. Wang, Y. Wang, W. W. Yu, *Adv. Mater.* **2016**, *28*, 10088.
- [175] S. Tu, Q. Yin, B. Shang, M. Chen, L. Wu, *Chem. Asian J.* **2019**, *14*, 3830.
- [176] F. Zhang, Z.-F. Shi, Z.-Z. Ma, Y. Li, S. Li, D. Wu, T.-T. Xu, X.-J. Li, C.-X. Shan, G.-T. Du, *Nanoscale* **2018**, *10*, 20131.
- [177] Y.-W. Zhang, G. Wu, H. Dang, K. Ma, S. Chen, *Ind. Eng. Chem. Res.* **2017**, *56*, 10053.
- [178] F. Palazon, F. Di Stasio, Q. A. Akkerman, R. Krahne, M. Prato, L. Manna, *Chem. Mater.* **2016**, *28*, 2902.

- [179] F. Palazon, Q. A. Akkerman, M. Prato, L. Manna, *ACS Nano* **2016**, *10*, 1224.
- [180] G. Volonakis, M. R. Filip, A. A. Haghighirad, N. Sakai, B. Wenger, H. J. Snaith, F. Giustino, *J. Phys. Chem. Lett.* **2016**, *7*, 1254.
- [181] C. N. Savory, A. Walsh, D. O. Scanlon, *ACS Energy Lett.* **2016**, *1*, 949.
- [182] W. Ke, C. C. Stoumpos, M. Zhu, L. Mao, I. Spanopoulos, J. Liu, O. Y. Kontsevoi, M. Chen, D. Sarma, Y. Zhang, M. R. Wasielewski, M. G. Kanatzidis, *Sci. Adv.* **2017**, *3*, e1701293.
- [183] I. Spanopoulos, W. Ke, C. C. Stoumpos, E. C. Schueller, O. Y. Kontsevoi, R. Seshadri, M. G. Kanatzidis, *J. Am. Chem. Soc.* **2018**, *140*, 5728.
- [184] W. Ke, C. C. Stoumpos, I. Spanopoulos, L. Mao, M. Chen, M. R. Wasielewski, M. G. Kanatzidis, *J. Am. Chem. Soc.* **2017**, *139*, 14800.
- [185] W. Ke, I. Spanopoulos, Q. Tu, I. Hadar, X. Li, G. S. Shekhawat, V. P. Dravid, M. G. Kanatzidis, *J. Am. Chem. Soc.* **2019**, *141*, 8627.
- [186] Y. Peng, Y. Yao, L. Li, Z. Wu, S. Wang, J. Luo, *J. Mater. Chem. C* **2018**, *6*, 6033.
- [187] M. I. Saidaminov, J. Almutlaq, S. Sarmah, I. Dursun, A. A. Zhumekenov, R. Begum, J. Pan, N. Cho, O. F. Mohammed, O. M. Bakr, *ACS Energy Lett.* **2016**, *1*, 840.
- [188] Y. Zhang, M. I. Saidaminov, I. Dursun, H. Yang, B. Murali, E. Alarousu, E. Yengel, B. A. Alshankiti, O. M. Bakr, O. F. Mohammed, *J. Phys. Chem. Lett.* **2017**, *8*, 961.
- [189] C. Zhou, Y. Tian, Z. Yuan, H. Lin, B. Chen, R. Clark, T. Dilbeck, Y. Zhou, J. Hurley, J. Neu, T. Besara, T. Siegrist, P. Djurovich, B. Ma, *ACS Appl. Mater. Interfaces* **2017**, *9*, 44579.
- [190] M. I. Saidaminov, O. F. Mohammed, O. M. Bakr, *ACS Energy Lett.* **2017**, *2*, 889.
- [191] M. R. Filip, S. Hillman, A. A. Haghighirad, H. J. Snaith, F. Giustino, *J. Phys. Chem. Lett.* **2016**, *7*, 2579.
- [192] Z. Xiao, K.-Z. Du, W. Meng, J. Wang, D. B. Mitzi, Y. Yan, *J. Am. Chem. Soc.* **2017**, *139*, 6054.
- [193] A. H. Slavney, L. Leppert, D. Bartesaghi, A. Gold-Parker, M. F. Toney, T. J. Savenije, J. B. Neaton, H. I. Karunadasa, *J. Am. Chem. Soc.* **2017**, *139*, 5015.
- [194] K. Du, W. Meng, X. Wang, Y. Yan, D. Mitzi, *Angew. Chem.* **2017**, *129*, 8270.
- [195] G. Volonakis, A. A. Haghighirad, R. L. Milot, W. H. Sio, M. R. Filip, B. Wenger, M. B. Johnston, L. M. Herz, H. J. Snaith, F. Giustino, *J. Phys. Chem. Lett.* **2017**, *8*, 772.
- [196] P. V. Kamat, J. Bisquert, J. Buriak, *ACS Energy Lett.* **2017**, *2*, 904.
- [197] K. M. McCall, C. C. Stoumpos, S. S. Kostina, M. G. Kanatzidis, B. W. Wessels, *Chem. Mater.* **2017**, *29*, 4129.
- [198] F. Giustino, H. J. Snaith, *ACS Energy Lett.* **2016**, *1*, 1233.
- [199] J. Luo, X. Wang, S. Li, J. Liu, Y. Guo, G. Niu, L. Yao, Y. Fu, L. Gao, Q. Dong, C. Zhao, M. Leng, F. Ma, W. Liang, L. Wang, S. Jin, J. Han, L. Zhang, J. Etheridge, J. Wang, Y. Yan, E. H. Sargent, J. Tang, *Nature* **2018**, *563*, 541.
- [200] F. Locardi, E. Sartori, J. Buha, J. Zito, M. Prato, V. Pinchetti, M. L. Zaffalon, M. Ferretti, S. Brovelli, I. Infante, L. De Trizio, L. Manna, *ACS Energy Lett.* **2019**, *4*, 1976.
- [201] N. N. K., A. Nag, *Chem. Commun.* **2018**, *54*, 5205.
- [202] A. Karmakar, G. M. Bernard, A. Meldrum, A. O. Oliynyk, V. K. Michaelis, *J. Am. Chem. Soc.* **2020**, *142*, 10780.
- [203] R. Gautier, M. Paris, F. Massuyeau, *J. Am. Chem. Soc.* **2019**, *141*, 12619.
- [204] G. Nedelcu, L. Protesescu, S. Yakunin, M. I. Bodnarchuk, M. J. Grotevent, M. V. Kovalenko, *Nano Lett.* **2015**, *15*, 5635.
- [205] B. R. Sutherland, E. H. Sargent, *Nat. Photonics* **2016**, *10*, 295.
- [206] M. M. Stylianakis, T. Maksudov, A. Panagiotopoulos, G. Kakavelakis, K. Petridis, *Materials* **2019**, *12*, 859.
- [207] G. Li, M. Price, F. Deschler, *APL Mater.* **2016**, *4*, 091507.



**Kangyu Ji** received his B.Eng. degree from Imperial College London in 2017 and then received his M.Phil. degree from the University of Cambridge in 2018. He is pursuing his Ph.D. degree at the University of Cambridge with research interests in perovskite light-emitting and imaging algorithm applications.



**Miguel Anaya** is a research fellow at Darwin College and a Marie Curie Fellow in the Cavendish Laboratory at the University of Cambridge. He completed his Ph.D. at the Spanish National Research Council in 2018, with recognition from the Spanish Royal Society of Physics as the Best Thesis in Experimental Physics. He leads a subgroup at the StranksLab focused on the modeling, fabrication, and characterization of perovskite-based light-emitting devices and sensors.



**Anna Abfalterer** graduated with a B.Sc. degree in chemistry from the University of Innsbruck, Austria. Supported by a Fulbright scholarship, she then received her M.Sc. degree in chemistry from the University of Minnesota – Twin Cities, USA. She is now a Ph.D. candidate at the University of Cambridge, focusing on the synthesis and characterization of lead-free perovskite-inspired materials for next-generation light-emitting applications.



**Samuel D. Stranks** is a university lecturer in energy and Royal Society University Research Fellow at the University of Cambridge. He completed his Ph.D. at Oxford University as a Rhodes Scholar followed by a Junior Research Fellowship at Worcester College, Oxford, and a Marie Curie Fellowship at MIT. His group's research focuses on the optical and electronic properties of emerging semiconductors for low-cost, transformative electronics applications including light-harvesting (e.g., photovoltaic) and light-emission (e.g., LED) devices. They use optical spectroscopic techniques to understand material and device photophysics on a range of length and time scales and relate these characteristics to local chemical, structural, and morphological properties.